https://doi.org/10.5194/wes-2025-98
Preprint. Discussion started: 17 June 2025

eawe european academy of wind energy
Open Access WIND ENERGY SCIENCE DISCUSSIONS

A wind turbine digital shadow for complex inflow conditions

Hadi Hoghooghi and Carlo L. Bottasso
Wind Energy Institute, Technical University of Munich, 85748 Garching b. München, Germany
Correspondence: Carlo L. Bottasso (carlo.bottasso@tum.de)

Abstract.

We present a digital shadow Kalman filtering approach based on the direct linearization of a multibody aeroservoelastic model of a wind turbine. In contrast to approaches based on ad hoc models, the reuse of existing trusted models reduces development time and duplication of effort, leverages resources invested in tuning and validation, and eventually increases confidence in the results.

This approach has already been pursued by others, but it is here improved with respect to several main aspects of the formulation. To extend the applicability to non-symmetric, waked, and yaw-misaligned conditions, the filter-internal model – in addition to the tower fore-aft and rotor rotational dynamics – now also includes the tower side-side and the flapwise and edgewise degrees of freedom of the rotor blades. To make the model aware of the inflow conditions at the rotor disk, inflow estimators are used to detect in real time during operation rotor-equivalent values of the wind speed, vertical shear, horizontal shear (on account of waked conditions), and yaw misalignment (in support of wake-steering control). These inflow parameters are used to schedule the filter-internal model, adapting its behavior to the current conditions experienced by the turbine. Furthermore, the filter-internal white-box model is augmented with data-driven corrections to improve its predictive accuracy. Two approaches are explored for the correction of the model: a bias correction method that attempts to improve both states and outputs, and a neural-based one that only corrects the outputs but not the states.

The proposed digital shadow is demonstrated first in a simulation environment, considering clean freestream, waked, and wake-steering conditions, and then using a field dataset collected on an instrumented turbine. To further validate its performance under complex inflow conditions, additional field data evaluations are conducted, including cases of extreme vertical shear, waked, and wake-steering conditions. Remarkably, the quality of the estimates of the damage equivalent loads for the field case is similar to the simulation case, even without any specific correction of the filter-internal model. However, after applying correction techniques, the quality of the estimates improves drastically, yielding errors in the damage equivalent load estimates of only a few percentage points.

1 Introduction

Digital twins for wind turbine applications have recently received a significant attention from the research community, on their way to become key components of modern wind systems. Digital twins can play various roles in multiple applications, including the support of control systems (Anand and Bottasso, 2023), the estimation of consumed and remaining lifetime

https://doi.org/10.5194/wes-2025-98
Preprint. Discussion started: 17 June 2025

eawe european academy of wind energy
Open Access WIND ENERGY SCIENCE DISCUSSIONS

(Branlard et al., 2020b; Song et al., 2023), and the monitoring of the condition of assets (Olatunji et al., 2021). In fact, wind turbines operate autonomously in complex, dynamic, and often harsh ambient conditions. The ability to mirror the behavior of each asset with its own digital replica clearly has a very significant potential and a wide scope. Additionally, by combining data with machine learning and artificial intelligence, the quality of the digital copy can be improved over time, with obvious benefits in productivity and profitability.

Digital twins provide services by building on the predictive abilities of digital shadows. In fact, a digital shadow is a mirror of an asset obtained through a one-way data flow (from physical asset to digital model), whereas a digital twin is based on a two-way data flow that closes the loop between the virtual and physical entities (Sepasgozar, 2021). This paper focuses on the formulation of a method to mirror the behavior of an asset, while the loop closure is not specifically considered here. Therefore, the term digital shadow, instead of digital twin, is preferred in the present context (Hoghooghi et al., 2024).

There is clearly a plethora of ways to develop digital shadows. Here, we expand on an approach based on the integration of an aeroservoelastic model of the machine with a Kalman filter (Grewal and Andrews, 2014; Branlard, 2019; Branlard et al., 2024a; Hoghooghi et al., 2024). Although this may seem to be a relatively standard and straightforward way of developing a digital shadow, it has a number of interesting characteristics. First, each wind turbine developer has trusted aeroservoelastic models of its turbines, which are fine-tuned during design and often carefully validated with data from instrumented prototypes and field trials. These models seem to be ideally suited for developing digital shadows instead of creating new ad hoc models from scratch for this specific task. Second, developing a digital shadow from an existing model immediately gives a baseline predictive ability, even in the absence of extensive field datasets. On the other hand, purely data-driven black-box approaches can only be aware of the informational content of the data they are trained on. Long measurement times may be needed for collecting datasets that cover all the operating conditions of interest (including the ones at the boundaries of the operational envelope) and that possess sufficient statistical significance, in turn hindering the applicability of methods that exclusively rely on data. From this point of view, an approach based on an existing trusted aeroservoelastic model seems to be more appealing, especially when considering that such a white model can later be turned into an adaptive grey model when augmented with corrective elements based on data.

The approach proposed here is based on the work of Branlard (2019) and Branlard et al. (2024a): an existing aeroservoelastic model is linearized around a number of operating conditions to define a linear state-space filter-internal model; at each time step, a Kalman filter is used to innovate the predictions of the model by using supervisory control and data acquisition (SCADA) measurements from the operating asset, delivering estimates of the model states and of additional outputs of interest.

This existing approach is improved here in four main ways.

First, in addition to the tower fore-aft and rotor rotational dynamics (Branlard, 2019; Branlard et al., 2024a), the filter-internal model now includes also the tower side-side and the flapwise and edgewise degrees of freedom (DOFs) of the rotor blades. This richer description of the system response is meant to enable the application of the digital shadow to more general operating conditions, as for example the ones in strongly sheared flows, or in wake overlap, or in yaw misalignment for wake-steering wind farm control.

https://doi.org/10.5194/wes-2025-98
Preprint. Discussion started: 17 June 2025

WIND ENERGY SCIENCE DISCUSSIONS

Second, because of the wider range of possible operating conditions now supported by the digital shadow, a more sophisticated scheduling of its linear state-space filter-internal model is necessary. To this aim, the model is scheduled here not only in terms of wind speed – as commonly done –, but also with respect to vertical shear, horizontal shear (on account of possible wake impingement), and yaw misalignment. These three extra scheduling parameters are tasked with informing the model of the current inflow conditions present at the rotor disk. These quantities are detected in real time during operation by dedicated observers (Kim et al., 2023; Bertelè et al., 2024).

Third, a bias-correction approach is used to improve the accuracy of the filter-internal model. The approach is designed to compensate for possible biases in the estimation of both the system states and of the output equations. To correct the system states, an error term is added to the dynamic force-balance equilibrium equations, and it is calibrated depending on the operating conditions. A more general approach would be to correct the state equations with a non-linear error term, following for example Bottasso et al. (2006). This is a planned future improvement, and in fact the implemented Kalman filter is already able to handle non-linear models (Wan and Van Der Merwe, 2000), but this capability is not discussed further here. To correct the output equations, measurement biases are promoted to state variables, whose dynamics are triggered by a dedicated process noise term. The approach is shown to yield a considerable improvement in the quality of the estimation of fatigue damage.

Fourth, the model is augmented by a data-driven learning element to improve its predictive ability for condition monitoring (CM) applications. In such a case, the correction is only applied to specific outputs of interest for which measurements are available. A neural-based correction term is added to the relevant model equations and trained based on the measurements provided by on-board sensors. After learning, the model achieves a very high accuracy in the predictions of these outputs, which a CM system (not described here) can leverage by comparing predictions with measurements in order to detect possible anomalies and faults.

The proposed approach is first demonstrated in a simulation environment under clean freestream, waked, and wake-steering conditions and then validated in the field using data from an instrumented multi-MW wind turbine, encompassing both clean and complex inflow conditions. The implementation is based on the widely used open-source aeroservoelastic simulation environment OpenFAST and associated tools (OpenFAST, 2024; Jonkman and Shaler, 2021; TurbSim, 2023), while the filter is based on MATLAB (The MathWorks, Inc., 2022). Clearly, the methodology is completely general and could be implemented in other software environments than the ones used here.

The literature on digital twins and their applications in wind energy is vast, especially on the topics revolving around structural fatigue (Bernhammer et al., 2016; Hoghooghi et al., 2019a, b). In fact, fatigue loads affect various wind turbine components – such as tower, blades, drivetrain, bearings, and others – causing permanent damage, in turn reducing lifetime, limiting revenue, and increasing operational costs (IEC, 2005; Hoghooghi, 2021). Consequently, fatigue reduction and lifetime estimation are areas of primary significance and interest for industry (Bottasso et al., 2013; Loew and Bottasso, 2022; Dimitrov et al., 2018). CM facilitates the real-time assessment of turbine health and performance, enabling proactive maintenance strategies to mitigate fatigue-induced failures and to optimize operational efficiency (Chen et al., 2016; Wu et al., 2021; Liu et al., 2023). Therefore, accurate fatigue estimation, coupled with effective CM practices, is essential for enhancing performance and reducing costs (Bangalore et al., 2017; Hoghooghi et al., 2020a, b, 2021; Surucu et al., 2023).

https://doi.org/10.5194/wes-2025-98
Preprint. Discussion started: 17 June 2025

The application of digital twin technology in condition monitoring and diagnosis offers numerous benefits. These include the optimization of fleet-wide performance, the continuous monitoring of critical components throughout their entire lifecycle, and the proactive planning of physical maintenance visits and repairs. Benefits also extend to other interesting applications, such as the training of maintenance engineers and technicians in virtual environments. All this has the potential for reduced costs, for improved availability by minimizing downtime, and for a faster and more effective identification of inefficiencies. Additionally, digital twins enable the forecasting of failure modes and their likely consequences, providing unique insights into the health of mechanical components of wind turbines (Olatunji et al., 2021). Intelligent monitoring procedures, a primary responsibility of digital twins, can be implemented directly (offline) or indirectly (online). Offline monitoring involves periodic machine-assisted onsite inspections, necessitating operational interruptions. In contrast, online monitoring entails a continuous monitoring of equipment via sensors during operation (Chen et al., 2016; Bangalore et al., 2017; Wu et al., 2021; Surucu et al., 2023).

There is also an ample literature on methods for estimating fatigue loads. For example, hybrid techniques that combine physics-based methods with SCADA data have been demonstrated by Noppe et al. (2016). Various other load estimation techniques have been described and successfully employed, including lookup tables (Mendez Reyes et al., 2019), modal expansion (Iliopoulos et al., 2016), ensemble aggregation of fatigue loads based on concurrent multiple simulations (Abdallah et al., 2017), machine learning (Evans et al., 2018), neural networks (NNs) (Schröder et al., 2018), polynomial chaos expansion (Dimitrov et al., 2018), deconvolution (Jacquelin et al., 2003), load extrapolation (Ziegler et al., 2017), virtual sensing based on reduced-order models (ROMs) extracted from finite element (FE) models (Vettori et al., 2020), and NN-based load surrogates (Guilloré et al., 2024).

This quick and necessarily incomplete overview of the vast literature on the subject gives an idea of the wide range of applications and benefits that digital twins may bring to the field. Yet, a successful digital twin must invariably rely on the modeling accuracy of its underlying digital shadow(s). The present work contributes to this important topic by formulating a procedure to develop digital shadows that leverage existing trusted multibody dynamics models, which often encapsulate a large body of experience and knowledge of wind turbine manufacturers. These models are linearized to increase computational efficiency and then augmented with flow estimators and learning elements, yielding simple-to-use yet effective and adaptive mirroring capabilities of wind assets in their full range of operating conditions.

The paper is organized as follows: Sect. 2 outlines the methodology, detailing the filter-internal model, its scheduling by inflow estimators, the correction of biases, and the a-posteriori data-driven adaptation of selected outputs. Section 3 characterizes the performance of the proposal digital shadow approach, first in a simulation environment considering clean freestream, waked, and wake-steering conditions, and then in the field using data from an instrumented multi-MW wind turbine, covering both clean and complex inflow conditions. Finally, Sect. 4 summarizes the key findings and outlines the next steps in this research.

https://doi.org/10.5194/wes-2025-98
Preprint. Discussion started: 17 June 2025

2 Methods

Figure 1 illustrates the key components of the proposed digital shadow workflow. A Kalman filter uses SCADA measurements to improve the predictions of a turbine ROM, in order to estimate the system states and other outputs of interest. The filter-internal model is obtained by linearization of a higher-fidelity multibody model of the turbine. Measurements of the blade loads are fused with the SCADA data stream to estimate some key characteristics of the inflow in real time during operation. In turn, these inflow parameters are used for the scheduling of the coefficients of the filter-internal model, thereby adjusting the filter behavior to the full range of operating and inflow conditions to which the turbine is exposed to.

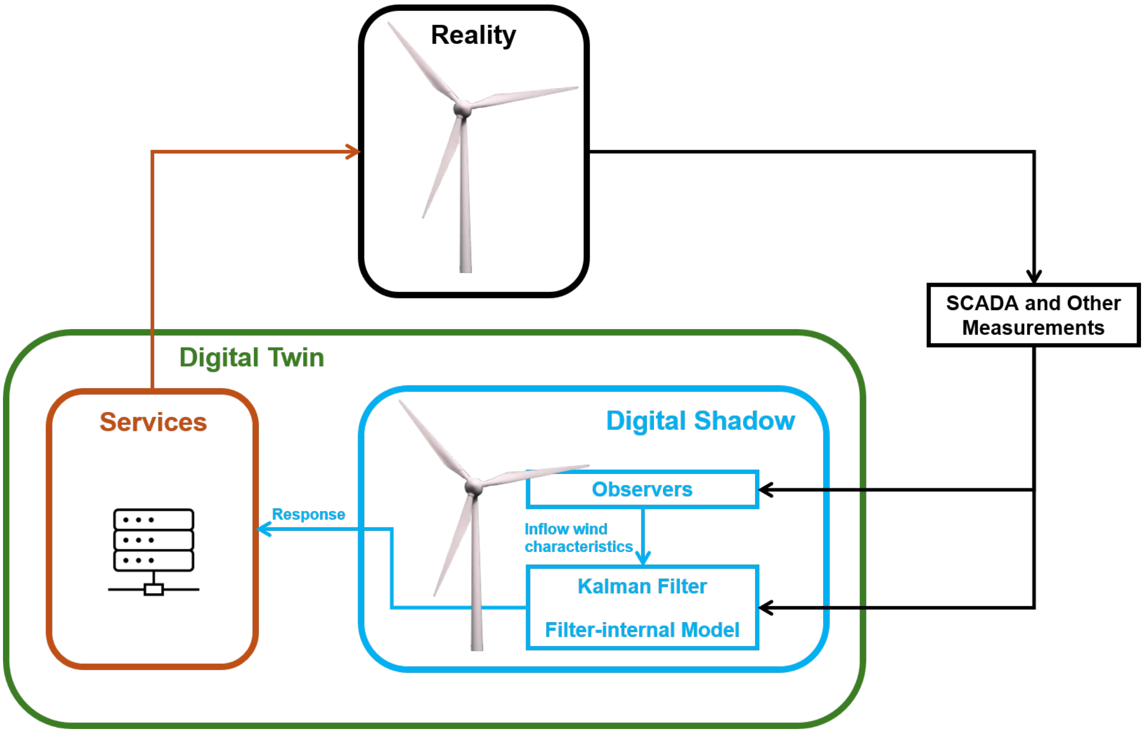

Figure 1. Schematic representation of the proposed digital shadowing approach.

2.1 Filter-internal model

We consider a non-linear multibody model of a wind turbine. The model is expressed in terms of the generalized displacements $\mathbf{q}$, generalized velocities $\mathbf{v}$, and inputs $\mathbf{u}$. Measurements affected by noise ν are available for the outputs $\mathbf{y}$, which are used by the filter to improve the prediction of the model states. Finally, $\mathbf{z}$ are additional output quantities of interest that do not participate in the filter innovation step.

The filter ROM is obtained by directly linearizing the non-linear multibody model around multiple equilibrium conditions where state, input, and output vectors are noted $\mathbf{q}_0$, $\mathbf{v}_0$, $\mathbf{u}_0$, $\mathbf{y}_0$, and $\mathbf{z}_0$. The resulting filter-internal linear model is written in

https://doi.org/10.5194/wes-2025-98
Preprint. Discussion started: 17 June 2025

terms of increments $\delta(\cdot)$ as

$$\delta\dot{\mathbf{q}} = \delta\mathbf{v}, \tag{1a}$$

$$\delta\dot{\mathbf{v}} = -\mathbf{M}^{-1}(\mathbf{C}\delta\mathbf{v} + \mathbf{K}\delta\mathbf{q} + \mathbf{U}\delta\mathbf{u} + \omega), \tag{1b}$$

$$\delta\mathbf{y} = \mathbf{D}_v\delta\mathbf{v} + \mathbf{D}_q\delta\mathbf{q} + \mathbf{E}\delta\mathbf{u} + \nu, \tag{1c}$$

$$\delta\mathbf{z} = \mathbf{F}_v\delta\mathbf{v} + \mathbf{F}_q\delta\mathbf{q} + \mathbf{G}\delta\mathbf{u}. \tag{1d}$$

The Kalman filter integrates these equations over time by first predicting the system state variables and their uncertainties and then correcting (innovating) these estimates using the available measurements, considering their associated uncertainties. Since the underlying model is linearized, the non-linear values of all quantities are obtained by adding the perturbations to the reference equilibrium conditions. For example, the generalized displacements are computed as $\mathbf{q} = \mathbf{q}_0 + \delta\mathbf{q}$, and the same holds for all other vectors appearing in Eqs. (1).

Equations (1a) are the kinematic relations, which are assumed to be exact and not affected by noise. Equations (1b) express the dynamic equilibrium of the system, affected by the process noise ω, where $\mathbf{M}$, $\mathbf{C}$, $\mathbf{K}$, and $\mathbf{U}$ are, respectively, the mass, damping, stiffness and control matrices. Finally, Eqs. (1c) and (1d) represent the linearized output equations for $\mathbf{y}$ and $\mathbf{z}$, respectively. The noise terms are assumed to be zero mean and uncorrelated (Grewal and Andrews, 2014).

It should be noted that the equilibrium conditions are, in general, periodic. As a result, the entries of the matrices associated with rotating quantities – as well as the associated states, inputs, and outputs – depend on time through the time-dependent azimuthal position of the rotor. To avoid working with periodic systems, this dependency is eliminated by averaging throughout a complete rotor revolution.

The present implementation considers 9 DOFs in the definition of the filter-internal dynamics. Accordingly, the generalized displacement vector is defined as

$$\mathbf{q} = \left\{d_T^{FA}, d_T^{SS}, \psi, d_{B1}^F, d_{B2}^F, d_{B3}^F, d_{B1}^E, d_{B2}^E, d_{B3}^E\right\}^T, \tag{2}$$

where d_T^{FA} and d_T^{SS} are the tower FA and SS deflections, respectively, ψ is the rotor azimuthal position, while d_{Bi}^F and d_{Bi}^E are respectively the flapwise and edgewise DOFs of the ith blade. The associated velocities are $\mathbf{v} = \dot{\mathbf{q}}$.

The input vector $\mathbf{u}$ contains 8 entries and it is defined as

$$\mathbf{u} = \{V, \alpha, \gamma, \theta_1, \theta_2, \theta_3, \theta_{\text{coll}}, Q_{\text{gen}}\}^T, \tag{3}$$

where V is the wind speed, α is the vertical power-law shear exponent, γ is the misalignment angle, θ_i is the total blade pitch angle of the ith blade, θ_{coll} is the collective blade pitch angle, and Q_{gen} indicates the generator torque. Individual pitch control adds to the ith blade an extra amplitude $\theta_i - \theta_{\text{coll}}$ with respect to the collective value, whereas $\theta_i = \theta_{\text{coll}}$ when only collective pitch is used. Notice that the input to the model not only considers the control inputs (i.e., quantities commanded by the on-board control system) but also includes exogenous terms due to the ambient conditions. The present inputs are relevant to the linearization performed in OpenFAST (Jonkman et al., 2018; NREL Forum), although other codes might use different quantities; for example, we note the presence of the vertical shear but not of the horizontal one.

https://doi.org/10.5194/wes-2025-98
Preprint. Discussion started: 17 June 2025

eawe european academy of wind energy
Open Access WIND ENERGY SCIENCE DISCUSSIONS

It is assumed that a biaxial accelerometer measures accelerations at the tower top, an encoder measures the rotor speed, and load measurements are available for each blade in the form of flapwise and edgewise bending moment components. Accordingly, the output vector $\mathbf{y}$ contains 9 entries and it is defined as

$$\mathbf{y} = \left\{\ddot{d}_T^{FA}, \ddot{d}_T^{SS}, \dot{\psi}, m_{B1}^F, m_{B2}^F, m_{B3}^F, m_{B1}^E, m_{B2}^E, m_{B3}^E\right\}^T. \tag{4}$$

The FA and SS tower top accelerations are $\ddot{d}_T^{FA}$ and $\ddot{d}_T^{SS}$, respectively, the rotor angular speed is $\dot{\psi} = \Omega$, while the flapwise and edgewise bending components for the ith blade are noted m_{Bi}^F and m_{Bi}^E, respectively.

The model is completed by the definition of additional to-be-estimated quantities $\mathbf{z}$, which, however, do not participate in the filter innovation step. This is because of two possible reasons:

- the digital shadow operates as a virtual sensor, as measurements of these quantities are not available through physical sensors (because of technical or economic reasons);
- the digital shadow supports a condition monitoring system that compares predictions with measurements in order to detect anomalies and faults.

Both of these scenarios are illustrated later in this work. Here the $\mathbf{z}$ outputs are represented by the components m_{TB}^{FA} and m_{TB}^{SS} of the bending moment at tower base and by the components $m_{Bi-15\%}^F$ and $m_{Bi-15\%}^E$ of the bending moment at 15% span of each blade; however, other choices are clearly possible, depending on need.

2.2 Model scheduling

To be usable in practice, the filter-internal model is scheduled as a function of a small set of parameters $\mathbf{s}$, chosen to capture the equilibrium operating condition about which linearization is performed. As a result, all matrices appearing in the state-space model expressed by Eqs. (1) depend on $\mathbf{s}$. For example, considering the mass matrix, $\mathbf{M} = \mathbf{M}(\mathbf{s})$, and the same holds for all other matrices. Similarly, all states, inputs, and outputs at the equilibrium condition depend on $\mathbf{s}$. For example, considering the generalized displacements, $\mathbf{q}_0 = \mathbf{q}_0(\mathbf{s})$, and the same holds for all other vectors.

The vector of scheduling parameters is defined as

$$\mathbf{s} = \{V, \alpha, k_h, \gamma\}^T. \tag{5}$$

The first two entries express the dependency of the model coefficients and equilibrium reference values on the ambient conditions through the wind speed V and the vertical power-law shear exponent α. The third entry is the linear horizontal shear k_h, on account of the possible presence of impinging wakes shed by upstream turbines. The fourth entry is γ, the yaw misalignment angle, included here to support wake-steering conditions for wind farm control.

The purpose of the scheduling vector of parameters is to make the model (and, hence, the filter) aware of the operating conditions that affect the turbine response; these effects would otherwise be lost when moving from the full non-linear model to its linearization.

https://doi.org/10.5194/wes-2025-98
Preprint. Discussion started: 17 June 2025

eawe european academy of wind energy
Open Access WIND ENERGY SCIENCE DISCUSSIONS

The non-linear model is linearized at a preselected set of discrete values of $\mathbf{s}$, chosen to cover the entire range of operative and ambient conditions of the machine. The corresponding matrices and equilibrium states, inputs and outputs are stored in look-up tables (LUTs). To express the dependency of the model on the linearization point, at run time, the current value of the scheduling vector $\mathbf{s}$ is estimated at each time instant by dedicated observers as explained in Sect. 2.3, and the model matrices are interpolated accordingly. The equilibrium values of states, inputs and outputs are similarly interpolated, which allows for the transformation of the filter-predicted incremental values into their non-linear corresponding quantities.

2.3 Observers

As previously explained, the filter-internal model coefficients are scheduled with respect to the parameters $\mathbf{s}$ that capture the current operating conditions. These parameters are chosen here as the wind speed, the vertical and horizontal shears, and the misalignment angle.

These quantities are estimated at each instant of time during operation and used to inform the filter-internal model of the current conditions. The present sequential implementation – where observers feed information to the Kalman filter – is clearly not the only option. Alternatively, one could have included the estimation of $\mathbf{s}$ in an expanded Kalman filter. The sequential approach was chosen here purely for simplicity and because legacy implementations of the observers were already available (Hoghooghi et al., 2024).

Regarding the misalignment, we note that its actual value can differ significantly from the commanded one. Therefore, here, we prefer to estimate γ through an observer rather than using the values requested by the on-board controller.

2.3.1 Simple wind speed observer

A rotor-equivalent wind speed is obtained by inverting the expression of the power coefficient:

$$C_p(\theta_{\text{coll}}, \lambda) = \frac{Q_{\text{aero}}\Omega}{0.5\rho A V^3}, \tag{6}$$

where $\lambda = \Omega R/V$ is the tip-speed ratio, R is the rotor radius, $A = \pi R^2$ is the rotor swept area, Q_{aero} is the aerodynamic torque, and ρ indicates the air density. The power coefficient C_p is computed by executing dynamic simulations with the full aeroservoelastic turbine model in constant wind speeds for a reference density ρ_{ref}. Sufficient time is allowed for the transient response to subside, and afterwards, the response is averaged over a few rotor revolutions to compute the relevant steady-state quantities. The results are stored in a LUT, yielding an expression for the rotor-equivalent wind speed as a function of pitch, rotor speed, aerodynamic torque, and density:

$$V = \text{LUT}_{C_p}(\theta_{\text{coll}}, \Omega, Q_{\text{aero}}, \rho/\rho_{\text{ref}}). \tag{7}$$

At run time, the LUT is used to obtain an estimate V_E of the rotor-equivalent wind speed. The current pitch setting θ_{coll} and rotor speed Ω are measured by the corresponding on-board sensors. The aerodynamic torque is computed as $Q_{\text{aero}} \approx Q_{\text{gen}} + J\dot{\Omega}$, where Q_{gen} is the measured generator torque, and the angular acceleration $\dot{\Omega}$ is obtained by numerically differentiating the rotor speed, J being the rotor inertia. Finally, density ρ is computed using the gas law from temperature.

https://doi.org/10.5194/wes-2025-98
Preprint. Discussion started: 17 June 2025

eawe european academy of wind energy
Open Access WIND ENERGY SCIENCE DISCUSSIONS

2.3.2 Shear and misalignment observers

The estimation of the horizontal and vertical shears and of the wind misalignment is obtained by the "rotor as a sensor" technology (see Kim et al. (2023); Bertelè et al. (2024) and references therein). This method exploits the fact that each of these inflow characteristics leaves a specific trace in the load response of a wind turbine. Leveraging this fact, one can then "invert" the measured response to infer these inflow quantities.

In this work, we use a version of the rotor as a sensor based on load harmonic amplitudes (Kim et al., 2023; Bertelè et al., 2024). In a nutshell, the estimator is formulated as

$$c_E = NN(\mathbf{p}, \mathbf{i}_M), \tag{8}$$

where c_E is an estimated wind inflow characteristic (either the vertical power-law shear coefficient α, the horizontal linear shear coefficient k_h, or the yaw misalignment angle γ), $NN(\cdot,\cdot)$ is a single-output NN with free parameters $\mathbf{p}$, and $\mathbf{i}_M$ is a vector of measured NN inputs. A different NN is used for each one of the three inflow parameters of interest. The input vector is defined as $\mathbf{i}_M = \{\mathbf{m}^T, V, \rho\}^T$, where $\mathbf{m}$ is a vector of harmonic amplitudes of the blade loads. For the estimation of shears and misalignment, it is enough to limit the harmonics to the one per rev (1P) components (Kim et al., 2023; Bertelè et al., 2024). Accordingly, vector $\mathbf{m}$ is defined as

$$\mathbf{m} = \{m_{1c}^{OP}, m_{1s}^{OP}, m_{1c}^{IP}, m_{1s}^{IP}\}^T, \tag{9}$$

where the subscripts $(\cdot)_{1c}$ and $(\cdot)_{1s}$ respectively indicate 1P cosine and sine terms, while the superscripts $(\cdot)^{OP}$ and $(\cdot)^{IP}$ indicate out and in-plane load components, respectively. The out and in-plane load components are referred to the rotor disk, and they are obtained by transforming the flapwise and edgewise components measured by the blade-attached sensors based on the current blade pitch setting.

The present implementation is based on a simple single-hidden-layer feed-forward neural network with sigmoid activation functions. The free network parameters $\mathbf{p}$ are trained by backpropagation with Bayesian regularization to reduce the chances of being trapped in local minima (Matlab, 2023; Burden and Winkler, 2009). Training is based on simulations conducted with the full aeroelastic model of the turbine using OpenFAST (OpenFAST, 2024). At each time step, the inflow quantities (shears and misalignment) are extracted from the TurbSim (TurbSim, 2023) turbulent flow field by best-fitting over the rotor disk area. Load harmonics are obtained from the blade root sensors via the Coleman-Feingold transformation (Coleman and Feingold, 1958) and then filtered to remove any remaining spurious noise.

At run time, Eq. (8) is used to produce estimates of the inflow quantities based on measured load harmonics, on the current rotor-equivalent wind speed from Eq. (7), and on air density ρ.

2.4 Model error correction

In general, some mismatch between the plant and the filter-internal model is to be expected, and this will invariably affect the performance of the digital shadow. The effects of model mismatches can be mitigated in various ways, such as by the tuning of

https://doi.org/10.5194/wes-2025-98
Preprint. Discussion started: 17 June 2025

the model parameters, by the dynamic data-driven adaption of the model (Anand and Bottasso, 2023; Bottasso et al., 2006), by the correction of biases (Chui and Chen, 1999; Drécourt et al., 2006; Grewal and Andrews, 2008), or by adapting the process noise term to capture the effects of unmodelled physics, among others (Branlard et al., 2020a). Here, we explore two methods: a bias-correction approach and a data-driven correction limited to the output equations.

2.4.1 Bias correction

First, we consider the correction of biases, intended as additive errors in the model. To this end, the filter-internal model expressed by Eqs. (1) is modified as

$$\delta\dot{\mathbf{q}} = \delta\mathbf{v}, \tag{10a}$$

$$\delta\dot{\mathbf{v}} = -\mathbf{M}^{-1}(\mathbf{C}\delta\mathbf{v} + \mathbf{K}\delta\mathbf{q} + \mathbf{U}\delta\mathbf{u} + \mathbf{f}_0 + \omega), \tag{10b}$$

$$\dot{\mathbf{b}} = \omega_b, \tag{10c}$$

$$\delta\mathbf{y} = \mathbf{D}_v\delta\mathbf{v} + \mathbf{D}_q\delta\mathbf{q} + \mathbf{E}\delta\mathbf{u} + \mathbf{b} + \nu, \tag{10d}$$

$$\delta\mathbf{z} = \mathbf{F}_v\delta\mathbf{v} + \mathbf{F}_q\delta\mathbf{q} + \mathbf{G}\delta\mathbf{u}. \tag{10e}$$

With respect to Eqs. (1), the model is modified to include two corrections.

The first is represented by the static force $\mathbf{f}_0$, which induces a steady extra deflection in the generalized displacements, meant to correct possible biases. As for all other terms in the model, also $\mathbf{f}_0$ is assumed to depend on the operating condition through the vector of scheduling parameters $\mathbf{s}$.

A second modification is obtained by introducing the term $\mathbf{b}$ in the output Eq. (10d), on account of possible biases in the sensors. Following a standard bias correction approach (Chui and Chen, 1999; Drécourt et al., 2006; Grewal and Andrews, 2008), the extra term $\mathbf{b}$ is promoted to a new state variable undergoing a random walk excited by the process noise ω_b, as expressed by Eq. (10c).

It should be noted that the two correction terms may compete with each other, and it might not always be possible to disentangle the effects of one from the effects of the other. In fact, a correction on the generalized displacements performed by $\mathbf{f}_0$ will in turn correct the outputs through the $\delta\mathbf{q}$ term in Eq. (10d), eventually affecting $\mathbf{b}$. To cope with the possible collinearity of these two corrections, $\mathbf{f}_0$ is first calibrated by neglecting $\mathbf{b}$ from the model. Once suitable values for $\mathbf{f}_0$ for varying $\mathbf{s}$ have been obtained, then $\mathbf{f}_0$ is frozen and the bias $\mathbf{b}$ is activated in the filter. This two-step process is demonstrated later on. In the interest of simplicity, one can instead neglect $\mathbf{f}_0$ and only use the extra $\mathbf{b}$ states, implicitly accepting that the displacements might be in error. Additionally, one can iterate between calibrating $\mathbf{f}_0$ and $\mathbf{b}$, adjusting both corrections to achieve better accuracy.

It is worth mentioning that the tuning of the model is performed based solely on the measured outputs $\mathbf{y}$, as in general measurements of the states or biases are not available.

https://doi.org/10.5194/wes-2025-98
Preprint. Discussion started: 17 June 2025

eawe european academy of wind energy
Open Access WIND ENERGY SCIENCE DISCUSSIONS

2.4.2 A posteriori error correction for condition monitoring applications

Next, we consider a case relevant to CM applications. In this scenario, the digital shadow is tasked with predicting the behavior of some quantities of interest. However, measurements are available for these same quantities at run time. A CM system can then exploit this redundancy by comparing predictions and measurements in order to detect faults or anomalies. Clearly, for such a system to work in an effective manner, the digital shadow predictions must be in very close agreement with the measurements in all nominal operating conditions. In general, such a close match is not possible by the use of the model expressed by Eqs. (1).

To achieve the desired accuracy between predictions and measurements, the linearized output equations for $\mathbf{z}$ (Eq. 1d) are augmented with a correction term ϵ:

$$\delta\mathbf{z} = \mathbf{F}_v\delta\mathbf{v} + \mathbf{F}_q\delta\mathbf{q} + \mathbf{G}\delta\mathbf{u} + \epsilon. \tag{11}$$

For complete generality, the error correction term is assumed to depend on the states $\delta\mathbf{q}$ and $\delta\mathbf{v}$, inputs $\delta\mathbf{u}$ and scheduling parameters $\mathbf{s}$, and it is approximated using a neural network:

$$\epsilon = NN_\epsilon(\mathbf{p}_\epsilon, \mathbf{s}, \delta\mathbf{q}, \delta\mathbf{v}, \delta\mathbf{u}), \tag{12}$$

where $\mathbf{p}_\epsilon$ are the free network parameters.

Note that this approach does not attempt to correct the system governing dynamics expressed by Eq. (1b). This means that the filtered states will, in general, not precisely match the true plant states (which, typically, are also not known). Nonetheless, this approach can still deliver accurate estimates of the outputs of interest $\mathbf{z}$ when the correction term is trained to learn the measured outputs $\mathbf{z}_M$.

Here again, a simple single-hidden-layer feed-forward neural network is found to give the necessary accuracy. Training is based on backpropagation (Matlab, 2023). Weibull weighting is used to improve performance in the most probable operating conditions (Bangalore et al., 2017; Surucu et al., 2023; Anand and Bottasso, 2023).

3 Results

3.1 Simulation-based results

First, we investigate the performance of the proposed digital shadow framework in a simulation environment, using the IEA-3.4-130-RWT reference wind turbine (IEA3.37MW, 2023) as implemented in OpenFAST (OpenFAST, 2024). The complete aeroelastic model was linearized for wind speeds ranging from 5 to 25 $\mathrm{m\,s^{-1}}$ with increments of 1 $\mathrm{m\,s^{-1}}$, power-law vertical shear exponents spanning from 0 to 0.48 with increments of 0.12, horizontal shears ranging from -0.1 to 0.1 with increments of 0.1, and at yaw misalignments of $0°$ and $-30°$. The filter was implemented in MATLAB (The MathWorks, Inc., 2022), and its execution on a standard single-CPU laptop took of the order of 6 minutes for a 10-minute physical-time simulation at a step frequency of 100 Hz.

https://doi.org/10.5194/wes-2025-98
Preprint. Discussion started: 17 June 2025

Turbulent flow fields were generated with TurbSim (TurbSim, 2023), spanning wind speeds varying in the range 5–11 $\mathrm{m\,s^{-1}}$, with a vertical power-law shear exponent of 0.2, and turbulence intensities (TIs) of 6% and 18%. According to standards, simulations were conducted for a duration of 10 minutes and repeated for 6 distinct random seeds. Gaussian noise was added to each measurement signal to account for typical uncertainties affecting SCADA sensors (Branlard et al., 2020b, a), with the noise level set at 10% of the standard deviation of each signal. Damage equivalent loads (DELs) were computed by rainflow counting (Natarajan, 2022).

While various aspects of the digital shadow formulation are significant, the selection of the process and measurement covariance matrices, as well as the filtering of measurements, can strongly impact the accuracy of the estimates (Branlard et al., 2020a). The measurement covariance was based on the expected noise affecting the measurements. The process noise covariance was empirically tuned by a trial and error process to improve the accuracy of the estimates (Branlard et al., 2020a). The tuned covariance did not exhibit a significant dependence on wind speed and turbulence, eventually delivering a consistent performance across all considered conditions.

3.1.1 Estimation of wind speed and shears

We start by verifying the accuracy of the estimates of wind speed and shear, which are used to schedule the model coefficients. Reference (ground truth) values were obtained at each instant of time from the TurbSim longitudinal components of the wind field: speed was obtained by averaging over the rotor disk, while shears by interpolating over the same rotor disk area a power law in the vertical direction and a linear function in the horizontal one.

Figure 2 compares the reference rotor-average wind speed (dashed blue line) with the estimated rotor-equivalent wind speed V_E from Eq. (7) (solid red line) for one of the simulations conducted in region II at a wind speed of 7 $\mathrm{m\,s^{-1}}$ and TI equal to 6% (Fig. 2a) and 18% (Fig. 2b). For the calculation of the estimated rotor-equivalent wind speed, the rotor speed and torque signals were low-pass filtered using a fifth-order Butterworth filter with a -3 dB cutoff frequency of 8 rpm (Schreiber et al., 2020b), in order to eliminate higher-frequency turbine dynamics and measurement noise.

For the same condition, Fig. 2c shows time histories of the reference power-law vertical shear (dashed blue line) and its estimate obtained with Eq. (8) (solid red line). Figure 2d displays a time history of the reference linear horizontal shear (dashed blue line) and of its estimate from Eq. (8) (solid red line) for a wind turbine in full-waked conditions (as described later in Sect. 3.1.4). We demonstrate the behavior of the horizontal observer in this condition because wake meandering creates visible changes in the shear at the impinged turbine, whereas only very modest horizontal shear changes are typically observed in TurbSim ambient flow fields.

For the calculation of shears, the load harmonics were computed via the Coleman–Feingold transformation (Coleman and Feingold, 1958) from the corresponding measured signals, followed by low-pass filtering (Bertelè et al., 2021). The shear-observing network is also fed with the estimated wind speed V_E obtained from Eq. (7) and with air density (here assumed to be known, and therefore not estimated).

In all cases, the estimates track the ground-truth values reasonably well, although they fail to capture some of the higher frequency content. This is due to the fact that the rotor-equivalent wind speed is estimated through the response of the turbine,

https://doi.org/10.5194/wes-2025-98
Preprint. Discussion started: 17 June 2025

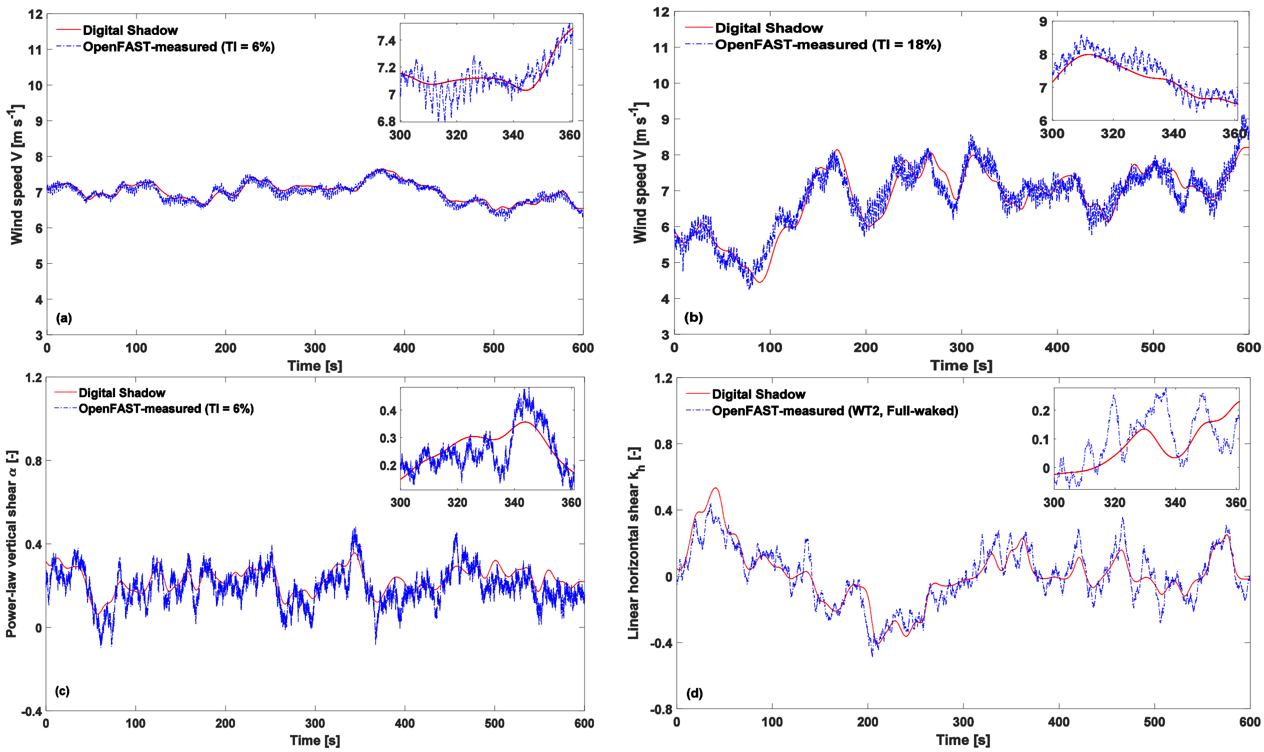

Figure 2. Time histories of the rotor-average wind speed from TurbSim and from Eq. (7) at a wind speed of 7 $\mathrm{m\,s^{-1}}$ and at TIs of 6% **(a)** and 18% **(b)**, respectively. **(c)**: time histories of the power-law vertical shear from TurbSim and from Eq. (8) a wind speed of 7 $\mathrm{m\,s^{-1}}$ and TI equal to 6%. **(d)**: time histories of the linear horizontal shear from TurbSim and from Eq. (8) for the downstream turbine in full-waked conditions (see Sect. 3.1.4). Reference results from TurbSim: dashed blue line; estimates: solid red line.

which is smoothed by the large inertia of the rotor and the presence of the control system. Similarly, the shear observers are driven by load harmonics, which here again entail some filtering of the higher frequency content of the blade response. Considering that these quantities are used for scheduling (i.e., interpolating) the system matrices and reference equilibrium conditions, the absence of some of the highest frequency components is probably an advantage more than a deficiency.

Over the entire range of simulations, the average absolute error was found to be 2.4% for wind speed, 14.5% for the vertical power-law shear exponent, and 11.1% for the linear horizontal shear. Furthermore, the average error for the mean yaw misalignment in the wake steering scenarios (described later in Sect. 3.1.4) was 14.5%.

3.1.2 Performance of the bias correction approach

To evaluate the BC approach described in Sect. 2.4.1 and to analyze the behavior of the two correction terms, we employed the same individual turbine operating in a clean low-TI inflow that was used in Sect. 3.1.1. Initially, the BC terms were switched off, yielding the baseline performance of the uncorrected approach. Figure 3a presents time histories of the tower top FA

https://doi.org/10.5194/wes-2025-98
Preprint. Discussion started: 17 June 2025

deflection as measured on the OpenFAST model (dashed blue line), uncorrected estimates from the digital shadow (solid red line), and corrected estimates using the BC approach (solid yellow line). These results correspond to a wind speed of 7 $\mathrm{m\,s^{-1}}$ and a turbulence intensity (TI) of 6%.

Introducing the static corrective force for the tower FA deflection, $\mathbf{f}_0^{FA}$, reduces the average absolute error from 16.4% to 2.5%. Figure 3b shows the variation of this static force with respect to the wind speed; the force is normalized to one at rated wind speed. Similar analyses were conducted for other DOFs, but are omitted here for brevity. It is worth noting that the small deviations observed between the linear and nonlinear models can be attributed to several factors, including shaft tilt, structural deflections, gravity loads, and slight discrepancies in azimuth angles due to minor differences in rotor speeds between the models (NREL Forum). Additionally, errors in the estimation of vector $\mathbf{s}$ contribute to the observed differences between the linear and nonlinear models.

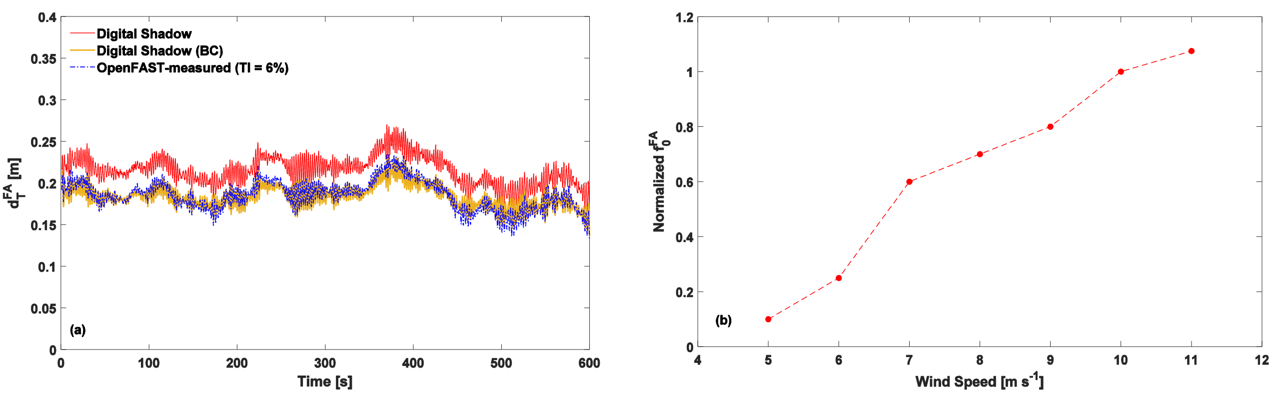

Figure 3. Time histories of tower top FA deflection as measured on the OpenFAST model (dashed blue line), uncorrected estimates from the digital shadow (solid red line), and corrected estimates using the BC approach (solid yellow line) at a wind speed of 7 $\mathrm{m\,s^{-1}}$ and a TI of 6% **(a)**. Variation of the static corrective force $\mathbf{f}_0^{FA}$ for the tower top FA deflection with respect to wind speed **(b)**. The static force is normalized to one at rated wind speed to highlight relative variations.

It is common to observe bias in one or more blade sensors (Pacheco et al., 2024). To demonstrate the effect of the term $\mathbf{b}$ in the correction of sensor biases (see Sect. 2.4.1, Eq. 10c), we artificially introduced a non-zero Gaussian noise in the strain gauge of blade 1, with a standard deviation of 0.01% and a mean equal to 10% of the mean value of the flapwise bending moment. Results are illustrated in Fig. 4a, where the OpenFAST unbiased model measurements are shown as a dashed blue line and the biased one as a dashed teal line. Figure 4b shows how the term $\mathbf{b}$ (dashed teal line) converges to the mean of the artificially added bias in the sensor (solid yellow line), effectively correcting the sensor output. Figure 4c shows the estimated blade 1 deflection measured on the OpenFAST model without bias (dashed blue line), with artificially introduced bias (dashed teal line), and the deflection estimated by the digital shadow using the BC approach (solid yellow line). The average absolute deflection error is 3.61% without the artificial bias and 3.67% with the compensated artificial bias, demonstrating that the

https://doi.org/10.5194/wes-2025-98
Preprint. Discussion started: 17 June 2025

eawe european academy of wind energy
Open Access
WIND ENERGY SCIENCE
DISCUSSIONS

correction is able to remove the problem without significant effects on the accuracy of the estimates. We also implemented this method for scenarios where each blade sensor was affected by a different bias, achieving a similar quality in the results.

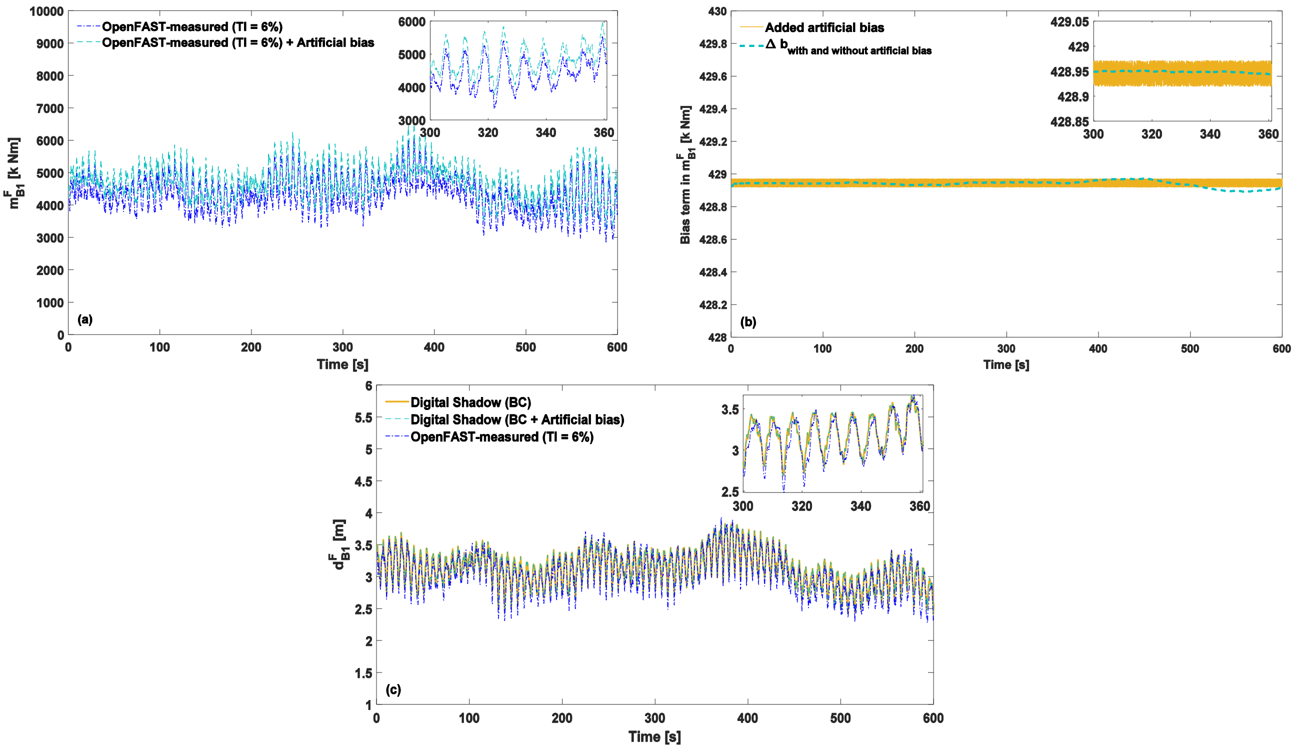

Figure 4. Time histories of blade 1 flapwise bending moment ($\mathbf{m}_F^{B1}$) as measured on the OpenFAST model without bias (dashed blue line) and with artificially introduced non-zero Gaussian noise (dashed teal line) **(a)**. Convergence of the term $\mathbf{b}$ (dashed teal line) to the mean of the artificially added bias (solid yellow line) **(b)**. Time histories the estimated blade 1 deflection as measured on the OpenFAST model without bias (dashed blue line), with artificially introduced non-zero Gaussian noise (dashed teal line), and as estimated by the digital shadow using the BC approach (solid yellow line) **(c)**. Results correspond to a wind speed of $7\,\mathrm{m\,s^{-1}}$ and a TI of 6%.

3.1.3 Application to an individual turbine

For the same individual turbine in clean low-TI inflow shown in Sect. 3.1.1, Fig. 5a through 5d report the time histories of the tower top FA and SS displacements, and the blade tip flapwise and edgewise deflections, respectively, as measured on the OpenFAST model (dashed blue line) and estimated by the digital shadow using BC (solid yellow line). Similarly, Fig. 5e and 5f report the time histories of the tower-base resultant bending moment and of the blade resultant bending moment at 15% blade span, respectively. Figure 5 reports a typical result, which was obtained with one single seed in region II at a wind speed of $7\,\mathrm{m\,s^{-1}}$ and TI equal to 6%. Table 1 gives a more complete overview of the performance of the digital shadow by reporting the average absolute errors for all conducted simulations.

https://doi.org/10.5194/wes-2025-98
Preprint. Discussion started: 17 June 2025

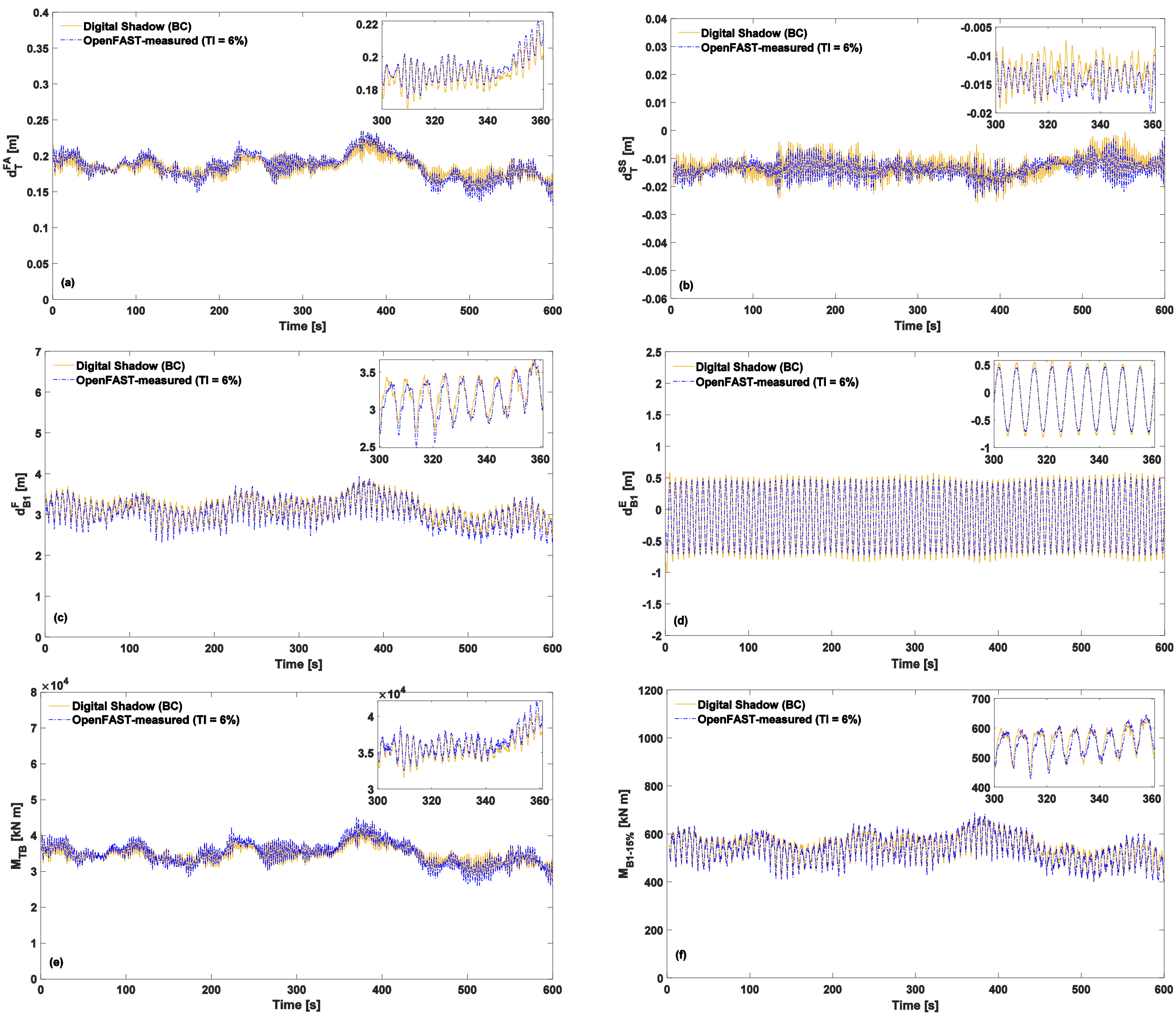

Figure 5. Time histories of tower top FA deflection **(a)**, tower top SS deflection **(b)**, and blade tip flapwise **(c)** and edgewise **(d)** deflections, tower-base bending moment **(e)**, and blade bending moment at 15% blade span **(f)**, as measured on the OpenFAST model (dashed blue line) and estimated by the digital shadow using BC (solid yellow line). A wind speed of 7 $\mathrm{m\,s^{-1}}$ and TI equal to 6% is considered.

https://doi.org/10.5194/wes-2025-98
Preprint. Discussion started: 17 June 2025

Table 1. Average absolute errors for all conducted simulations for clean inflow conditions.

Situation	Avg. estimation error [%]					
	d_T^{FA}	d_T^{SS}	d_B^F	d_B^E	M_{TB} DELs	$M_{B-15\%}$ DELs
No wake, TI=6%	3.1	1.7	3.8	4.4	5.1	12.2
No wake, TI=18%	6.9	3.5	5.6	6.0	6.9	13.0
Average	5.0	2.6	4.7	5.2	6.0	12.6

Results indicate that the average absolute errors of the estimated turbine states consistently remain below 10% across all conducted simulations. DELs were computed for the resultant moment at tower base, noted M_{TB}, and at 15% blade span, noted $M_{B-15\%}$. The average absolute errors for these two quantities are in the range of 5%–15%, with standard deviations averaging approximately 2.7% for M_{TB} and 4.5% for $M_{B-15\%}$ across all simulation scenarios. As expected, errors are larger for higher TI. The range of the average estimation errors is in line with the findings of previous studies (Abdallah et al., 2017; Branlard et al., 2020a, b, 2024a), which, however, used a smaller number of DOFs and did not consider blade dynamics.

3.1.4 Application to waked turbines in a small cluster

To assess the performance of the proposed method in more complex inflow conditions, simulations were conducted for a small cluster of wind turbines using FAST.Farm (OpenFAST, 2024). The cluster consists of three IEA 3.4-130 RWT turbines (IEA3.37MW, 2023) arranged in a row, as shown in Fig. 6, and named WT1, WT2, and WT3, from the upstream to the most downstream one.

Two different scenarios were considered:

- In the first case, the front turbine WT1 is aligned with the wind direction. The incoming wind is at rated speed ($9.8\,\mathrm{m\,s^{-1}}$) with a turbulence intensity of 6%. As a result, turbine WT2 is entirely within the wake of WT1, and WT3 is entirely within the wake of WT1 and WT2. The digital shadow is applied to the two downstream wake-affected turbines WT2 and WT3.

- In the second case, the ambient conditions are the same as in the first case, but the front turbine WT1 is misaligned by $-30°$ (i.e., pointing to the right when looking upstream) relative to the wind direction. Consequently, turbine WT2 is partially waked by WT1, while WT3 is fully within the wake of WT2 and partially in the one of WT1. The digital shadow is applied to the misaligned front turbine WT1, as well as to the two waked ones WT2 and WT3.

Table 2 presents an overview of the average absolute errors and the estimated output DELs for the two scenarios. For the waked and yawed turbines, the order of magnitude of the average estimation errors in the blade DELs is in line with the errors observed in Sect. 3.1.3 for the single turbine operating in a high TI freestream. However, the errors in the tower DELs are somewhat higher in both scenarios. Although the ambient turbulence here is only 6%, these results are consistent

https://doi.org/10.5194/wes-2025-98
Preprint. Discussion started: 17 June 2025

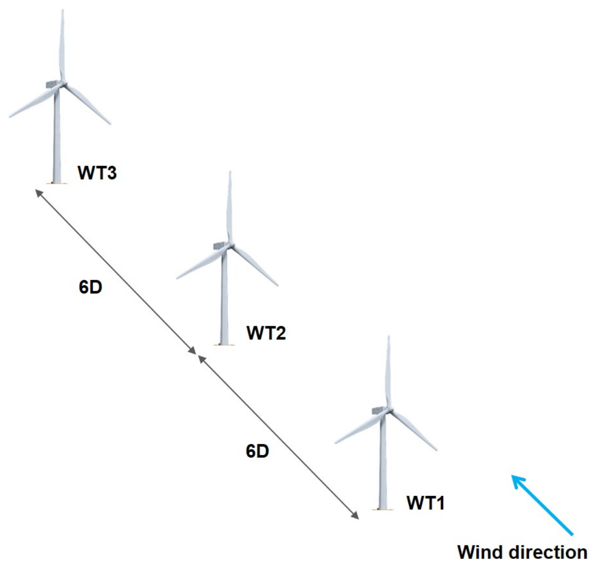

Figure 6. Layout of a small cluster of three IEA 3.4-130 RWT turbines. For all considered cases, the wind direction (indicated by the blue arrow) is parallel to the row of turbines.

with the effects of wake-added turbulence on the impinged turbines. While the errors in the tower DELs are similar for WT1 in misaligned conditions and for WT2 when partially waked, blade DELs are larger for the latter. This is likely due to the complex and asymmetrical inflow generated by the deflected wake on the impacted turbines and the ensuing complex response of the rotor blades.

Notwithstanding the low ambient turbulence, the errors in the tower DELs are somewhat larger for the front turbine when it is yawed, compared to the typical errors observed for the downstream waked turbines. This is likely due to the complex response of a yawed rotor, which is probably not accurately captured by the filter-internal model. In addition, even the blade element momentum (BEM) approach implemented in OpenFAST is not necessarily very accurate in such conditions (Branlard et al., 2024b), whereas computational fluid dynamics (CFD) and free vortex methods may be able to better render the underlying complex physics (Boorsma et al., 2018).

For a deeper insight into these results, Fig. 7a and 7c show the amplitude of the Fast Fourier Transform (FFT) of the tower-base bending and blade bending moment at 15% blade span, respectively, for a single turbine in clean inflow condition at a wind speed of $9\ \mathrm{m\,s^{-1}}$ and TI equal to 6%, while Fig. 7b and 7d show the same for WT2 in partially waked condition, with an observed average wind speed of $9\ \mathrm{m\,s^{-1}}$. The OpenFAST ground-truth measurements are shown with dashed blue lines, while the estimates are represented by solid yellow lines. All FFT amplitudes are normalized relative to the peak amplitude recorded by OpenFAST.

The digital shadow is capable of capturing reasonably well the overall trend of the spectrum as the turbine moves from an aligned to a misaligned condition for the frequencies clustered around the 1 to the 3P harmonics. The peaks of the OpenFAST-

https://doi.org/10.5194/wes-2025-98
Preprint. Discussion started: 17 June 2025

Table 2. Average absolute errors of the estimated outputs for all considered situations with complex inflow conditions, encompassing fully, partially, and overlapping waked conditions.

Scenario	Turbine	Condition	Avg. estimation error [%]	
			M_{TB} DELs	$M_{B-15\%}$ DELs
No wake steering	WT2	Fully waked	13.0	14.2
	WT3	Fully waked	10.1	13.4
Wake steering	WT1	Misaligned	16.1	13.4
	WT2	Partially waked	15.5	16.7
	WT3	Overlapping wakes	10.5	15.7
Average estimation error over all complex inflow conditions			13.0	14.7

measured tower-base and blade bending moments are approximately 5 and 3 times higher under waked conditions compared to the no wake condition. The errors in the peak amplitude of the tower-base bending moment are 14% under clean inflow conditions and 46% under waked conditions. Similarly, the errors in the peak amplitude of the blade bending moment are 18% for the clean inflow case and 34% for the waked condition.

Although the proposed digital shadow is clearly not providing an exact representation of the turbine behavior, the accuracy of the blade response in complex partially-waked and misaligned conditions is only slightly worse than the tower response provided by recent simpler digital shadows (Branlard et al., 2020b, 2024b), which would not be applicable in such non-symmetric conditions.

3.2 Validation against field measurements

Next, the digital shadow is tested in real-world conditions, using measurements obtained on a 3.5 MW eno wind turbine (eno energy GmbH). The available measurements include generator torque, rotor rotational speed, pitch angle, tower-top accelerations in both FA and SS directions, and blade root bending moments in the flapwise and edgewise directions. Additional strain gauges measure two components of the tower-base bending moment and of the blade bending moment at 25% blade span. All measurements are sampled at a rate of 10 Hz. We leverage these measurements for a dual purpose: in a first step, they are used to assess the quality of the predictions of the digital shadow, as discussed in Sect. 3.2.2; in a second step, they are used to train a data-driven correction of the corresponding output model using Eq. (11), as discussed later in Sect. 3.2.4.

Following the same approach described in Sect. 2.1, the filter-internal model is obtained by linearizing an existing OpenFAST model of the wind turbine across a predetermined range of operating conditions from cut-in to cut-out.

https://doi.org/10.5194/wes-2025-98
Preprint. Discussion started: 17 June 2025

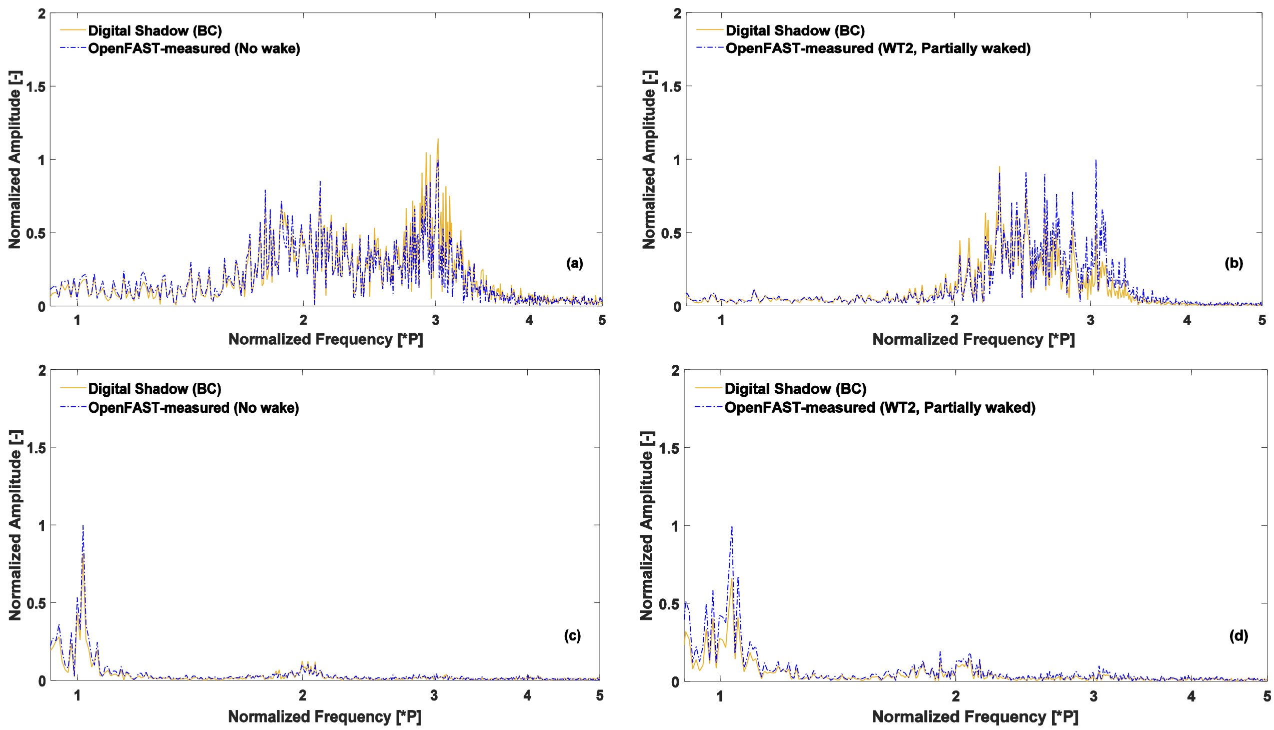

Figure 7. Spectra of the tower base bending moment (**a, b**) and the blade bending moment at 15% blade span (**c, d**) under clean inflow and partially waked conditions, respectively. The results are shown as measured on the OpenFAST model (dashed blue line) and as estimated by the digital shadow using BC (solid yellow line). The frequencies are normalized by the mean rotor speed, and all FFT amplitudes are scaled relative to the peak amplitude recorded by OpenFAST.

3.2.1 Test site

The dataset used in the current study was collected at a test site from 15 to 30 October 2020, and 23 to 26 February 2021 within the scope of a different project unrelated to the research described here. Measurements were used without applying any calibrations or adjustments and were filtered to eliminate gaps, stops, faults, or any other condition that does not represent a normal power production operating mode.

The test site, illustrated in Fig. 8, is located in northeast Germany, near the village of Kirch Mulsow, in the Rostock district of Mecklenburg-Vorpommern, a few kilometers from the Baltic Sea. The terrain comprises gentle hills, open fields, and forests. Four turbines, manufactured by eno energy GmbH (eno energy GmbH), are installed at the site. The digital shadow was applied to replicate the response of WT3. The main technical specifications of WT3 and WT4 are summarized in Table 4; WT1 and WT2 are not described further, as they played no role in the present experiment.

The testing period is classified into different inflow conditions, as presented in Table 3. After filtering to remove gaps and non-power production conditions, approximately 49 h of data were selected from the available measurement streams during

https://doi.org/10.5194/wes-2025-98
Preprint. Discussion started: 17 June 2025

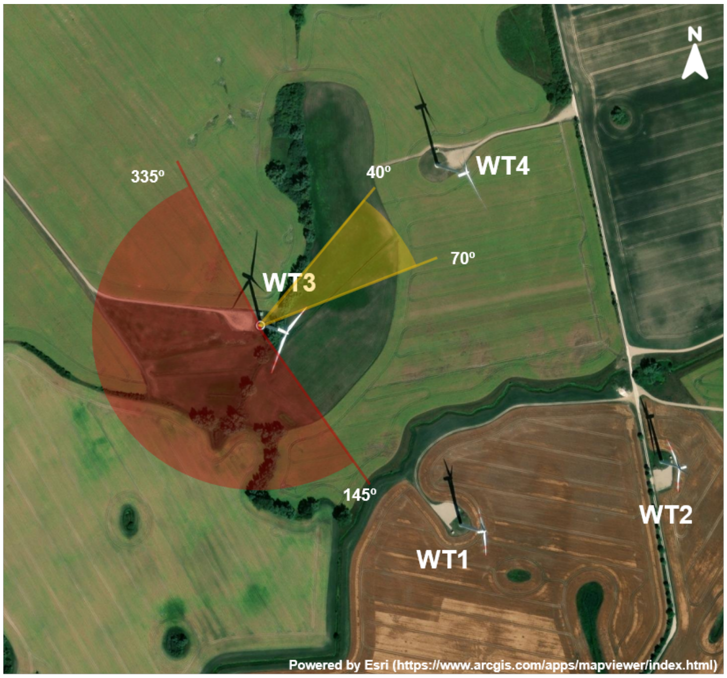

Figure 8. Layout of the test site, showing the turbine locations. The digital shadow is tested for the response of WT3. The sectors highlighted in red and yellow indicate the wind direction range during the testing period, which are characterized by clean freestream and waked conditions, respectively.

the testing period under clean free-stream conditions. The resulting dataset was divided into two subsets: the first, comprising 38 h (approximately 77% of the total), was used to train the correction approaches described in Sect. 2.4. The remaining 11 h were reserved for validation, representing a sample day with clean inflow conditions. In addition, as shown in Table 3, data from selected days with complex inflow conditions were used to further assess the performance of the digital shadow under complex inflow scenarios. It should be noted that no data from complex inflow conditions were used for tuning the correction terms discussed in Sect. 2.4.1.

Table 3. Inflow conditions during the testing period.

Inflow conditions	Specific conditions	Wind direction [°]	Time period	Total hours	Data split [hrs]
Clean freestream	Normal	145–335	17-31 Oct. 2020	49	38 (training) / 11 (testing)
Complex inflow	Extreme vertical shear	145–335	26 Oct. 2020	3	3 (testing)
	Wake steering via yaw control	200–230	23 Feb. 2021	2.5	2.5 (testing)
	Waked	40–70	15 Oct. 2020	2	2 (testing)

https://doi.org/10.5194/wes-2025-98
Preprint. Discussion started: 17 June 2025

eawe european academy of wind energy
Open Access WIND ENERGY SCIENCE DISCUSSIONS

Table 4. Technical specifications of the WT3 and WT4 turbines at the test site.

Wind turbine	Turbine specifications				
	Turbine model	Rotor diameter $[\mathrm{m}]$	Hub height $[\mathrm{m}]$	Rated power $[\mathrm{MW}]$	Cut-in, rated, cut-out speeds $[\mathrm{m\,s^{-1}}]$
WT3	eno126	126	117	3.5	3.0, 12.5, 25.0
WT4	eno126	126	137	3.5	3.0, 12.5, 25.0

Wind speed and shear estimators for these turbines were developed and validated in previous studies (Schreiber et al., 2020a; Bertelè et al., 2021).

3.2.2 Digital shadow performance without correction

First, we assess the ability of the digital shadow in estimating quantities of interest (in this case, loads), where no physical sensors are available. To this purpose, the digital shadow is fed with SCADA data, blade root load measurements, and the inflow quantities produced by the wind observers, but not with the tower-base and 25%-span blade measurements. Rather, these measurements are used to assess the quality of the estimates of the same quantities provided by the digital shadow.

Figure 9a and 9b report the time histories of the normalized measured (dashed blue line) and estimated (solid red line) tower-base bending moment resultant and blade bending moment resultant at 25% blade span, respectively, for $11\ \mathrm{h}$ on a sample day (20 October 2020) in the available dataset under clean freestream conditions. On this day, the turbine experienced clean inflow conditions with an average TI of 13.5%, as measured by the met mast.

Upon closer inspection of the zoomed-in insets of Fig. 9, it appears that the digital shadow is able to follow remarkably well both the high and low-frequency variations of the measurements. However, the estimated response also exhibits a clear offset. This is the effect of the approximate nature of the aeroelastic model, which creates a larger plant/internal-model mismatch in real-world conditions than in the simulated case analyzed in Sect. 3.1.3, where an identical OpenFAST model was used for defining the filter-internal model but also served as plant.

The average absolute errors for the tower-base and 25%-span blade bending moment resultants are found to be 5.9% and 21.3%, respectively, for the sample day shown in Fig. 9. Additionally, considering the training dataset, the average absolute error for the tower-base bending moment resultant is 12.4% (with a minimum of 9.7% and a maximum of 19.7%), while for the 25%-span blade bending moment resultant is equal to 18.7% (ranging between 13.7% and 23.7%).

3.2.3 Virtual sensing (bias correction)

Second, in order to remove the offset, the correction of both outputs and states is obtained with the BC approach described in Sect. 2.4.1 and based on Eqs. (10).

The empirical tuning of the correction terms was guided by the quality of the measurements at the tower top and blade root, utilizing the data streams available during the testing period, as described in Sect. 3.1.2. First, the static force term $\mathbf{f}_0$

https://doi.org/10.5194/wes-2025-98
Preprint. Discussion started: 17 June 2025

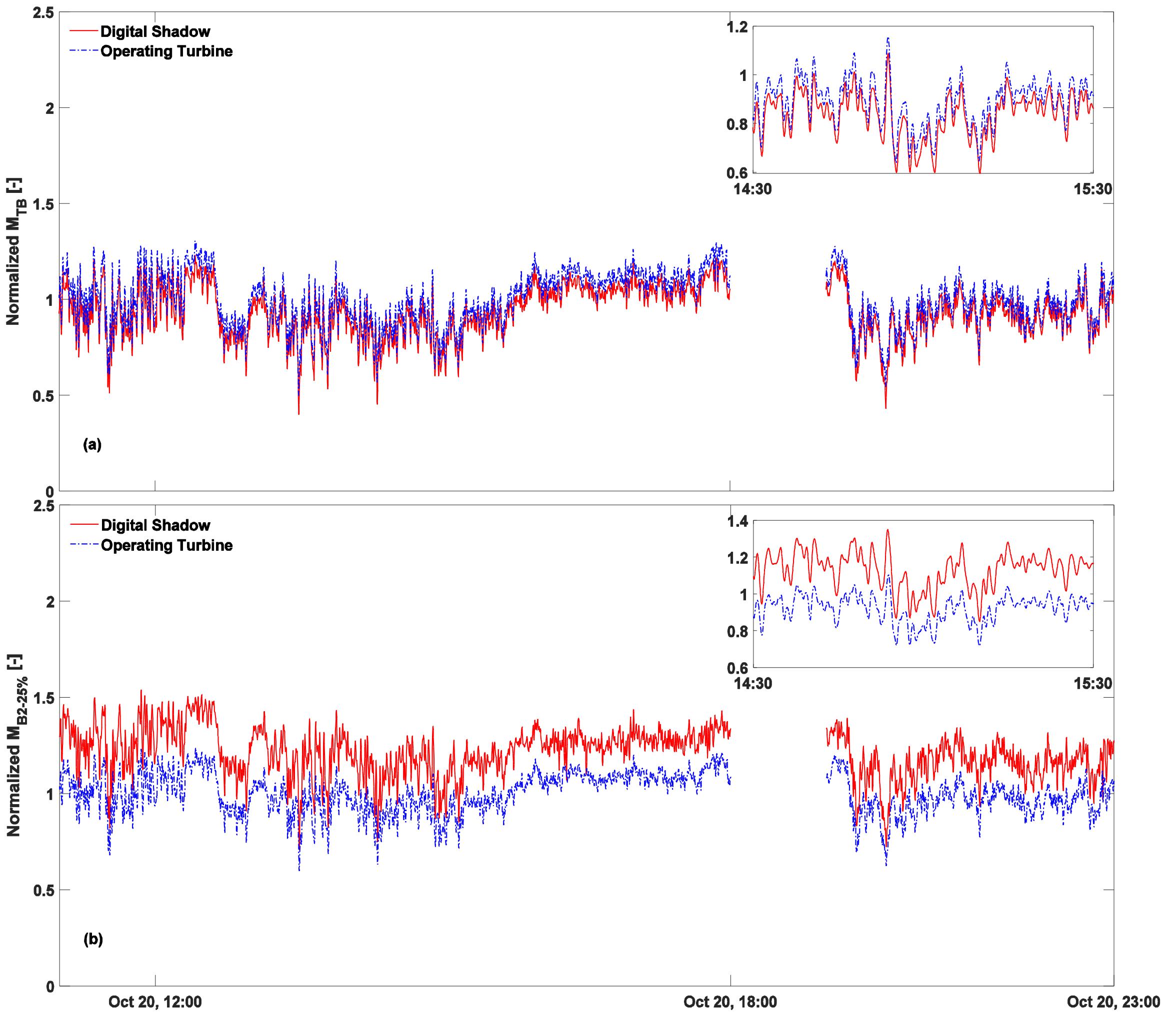

Figure 9. Time histories of tower-base bending moment **(a)** and blade bending moment at 25% blade span **(b)**, as measured (dashed blue line) and estimated by the digital shadow (solid red line) for 11 h on a sample day (20 October 2020) in the available dataset under clean freestream conditions. All values have been normalized using the same factor to preserve the confidentiality of the turbine data.

https://doi.org/10.5194/wes-2025-98
Preprint. Discussion started: 17 June 2025

was modified by trial and error until no further improvement was possible. It was found that this term depends primarily on wind speed, while the other terms of the scheduling set $\mathbf{s}$ had only a negligible effect for the data streams under clean freestream conditions. Next, the bias $\mathbf{b}$ was activated, and its driving process noise was calibrated to further reduce the error in the measurements. As for the process noise affecting the dynamic equilibrium equations, this calibration term again did not exhibit a significant dependency on wind speed or turbulence intensity. It should be noted that, considering the training dataset, after tuning, the average absolute error for the tower-top acceleration resultant is 3.1%, while it is 3.5% for the blade root bending moment resultant.

Table 5 presents an overview of the average absolute errors and the estimated output DELs for the complete dataset, categorized by the inflow conditions defined in Table 3.

After implementing the bias correction, the average absolute errors for M_{TB} and $M_{B-25\%}$ decreased to 4.2% and 2.7%, respectively, for the same sample day shown in Fig. 10, indicating that the offset in the estimations has been effectively removed. In addition, the DEL estimation errors for M_{TB} and $M_{B-25\%}$ became 4.3% and 9.1%, respectively. Overall, the BC approach seems to be capable of tracking both low- and high-frequency fluctuations in the quantities of interest, and of providing accurate estimates of their DELs.

It should be mentioned that the BC method appears to be more effective in correcting estimated quantities in the real field case than in the simulation environment. This could be due to several reasons, such as higher TI and a sampling rate that is ten times faster in the simulation case. In fact, the higher sampling rate introduces more high-frequency fluctuations, which are more challenging to estimate accurately.

Since the bias correction approach is a generalizable method and has demonstrated strong performance, the remaining results for complex inflow conditions are obtained using this approach. This decision is further motivated by one of the key applications of the digital shadow, which acts as a virtual sensor to estimate quantities that cannot be measured directly due to technical or economic limitations. To illustrate these results, time history plots are provided only for the waked inflow conditions (Fig. 11), as this scenario is particularly relevant and informative for understanding model behavior under complex aerodynamic interactions. Figures for other inflow conditions are omitted to maintain conciseness and avoid redundancy.

– ***Extreme vertical shear:***

The bias correction – tuned using the training dataset defined in Table 3 – was developed without using any data from complex inflow conditions. Despite this, the average absolute errors for M_{TB} and $M_{B-25\%}$ are 6.0% and 2.4%, respectively, for the dataset corresponding to the extreme vertical shear scenario defined in Table 3. Additionally, the DEL estimation errors for M_{TB} and $M_{B-25\%}$ are 6.7% and 7.3%, respectively, demonstrating the ability of the BC approach to provide estimations with errors below 10%, even under extreme shear conditions. It should be noted that the power law vertical shear ranges from 0.15 to 0.72, with an average value of 0.42.

– ***Wake steering via yaw control:***

For the dataset corresponding to the wake steering via yaw control scenario defined in Table 3, the average absolute errors for M_{TB} and $M_{B-25\%}$ are 6.2% and 2.3%, respectively. Additionally, the DEL estimation errors for M_{TB} and $M_{B-25\%}$ are 0.9%

https://doi.org/10.5194/wes-2025-98
Preprint. Discussion started: 17 June 2025

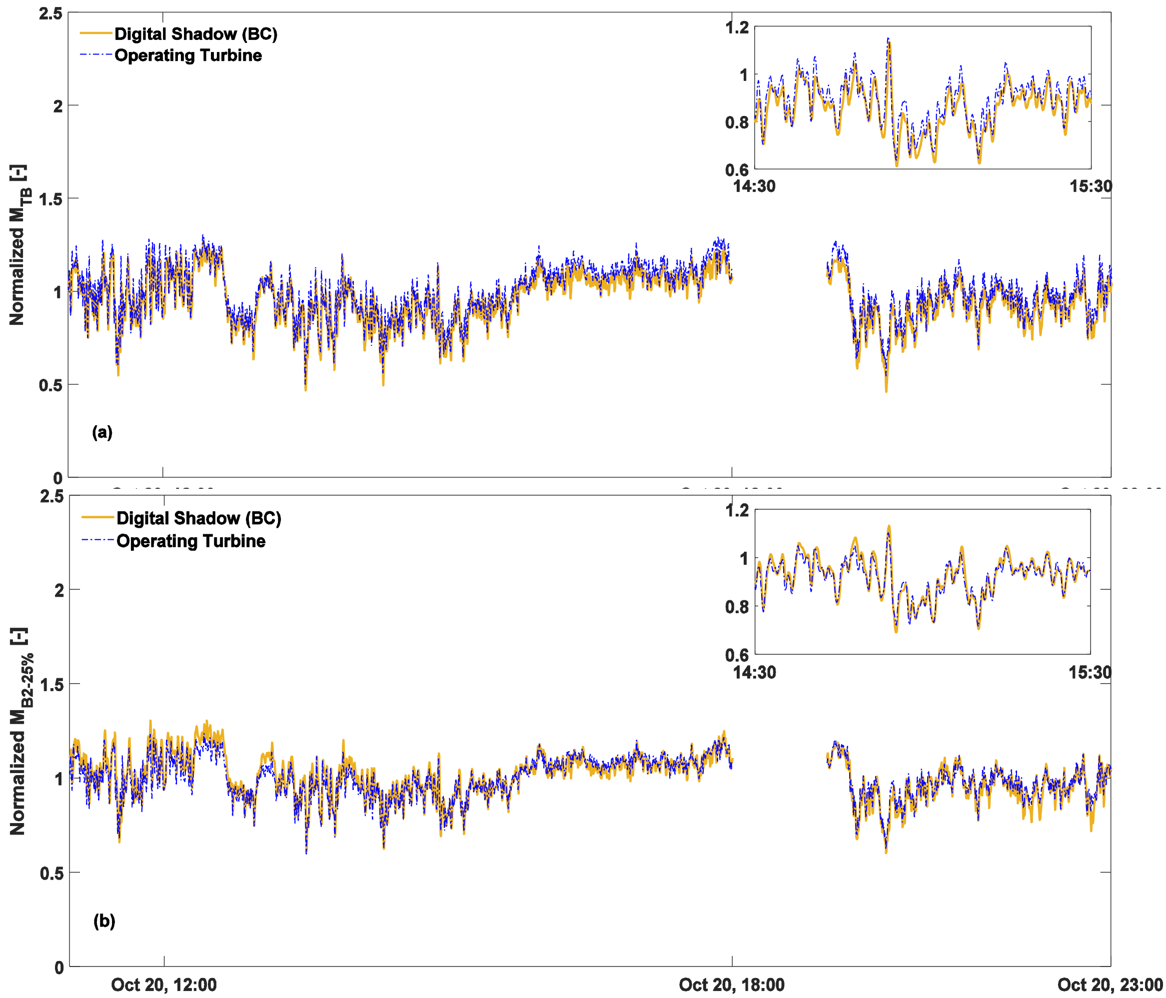

Figure 10. Time histories of the tower-base bending moment **(a)** and blade bending moment at 25% blade span **(b)** for 11 h on a sample day (20 October 2020) in the available dataset under clean freestream conditions. Measurements: dashed blue line; corrected estimates of the digital shadow using BC: solid yellow line. All values have been normalized using the same factor to preserve the confidentiality of the measured turbine data.

and 8.0%, respectively, with yaw misalignment ranging from $-16°$ to $11°$. It is important to note that the turbine dynamics in wake steering control mode are inherently more complex, further highlighting the performance of the digital shadow under complex inflow conditions.

540 – ***Waked:***

Figures 11(a), 11(b), 11(c), and 11(d) present the time histories of the tower-base bending moment, 25%-span blade bending moment resultants, and vertical and horizontal shears, respectively, for the dataset corresponding to the waked scenario defined

https://doi.org/10.5194/wes-2025-98
Preprint. Discussion started: 17 June 2025

in Table 3. Measurements are indicated by a dashed blue line, while the fine-tuned BC-corrected values are shown with a solid yellow line. As illustrated in Fig. 11(c), the power law vertical shear has an average value of -0.15, marked by a dark red dashed line. This condition is attributed to the higher hub height of WT4 and the influence of its wake on WT3. Furthermore, as shown in Fig. 11(d), the horizontal shear – indicated by a light red dashed line – has an average value of -0.12, further confirming the presence of waked conditions on WT3.

The average absolute errors for M_{TB} and $M_{B-25\%}$ are 11.4% and 5.1%, respectively, while the DEL estimation errors are 0.9% and 13.3%, respectively, for the dataset presented in Fig. 11. These results indicate that, while the BC approach generally performs well, the inherently complex turbine dynamics and the significant variations in vertical and horizontal shear under wake conditions contribute to the observed discrepancies, resulting in errors slightly exceeding 10%.

Overall, the range of average estimation errors is consistent with the findings of previous studies (Abdallah et al., 2017; Branlard et al., 2020a, b, 2024a), which, however, used a reduced number of degrees of freedom (DOFs), did not account for blade dynamics, and were not validated under complex inflow conditions.

However, the slightly higher estimation errors observed under complex inflow conditions suggest that, while the model is effective, further refinement using a larger dataset may be necessary to reduce residual offsets and achieve more accurate predictions in such scenarios. Additionally, the tuning of the BC correction term could be enhanced by incorporating not only wind speed but also variations in vertical and horizontal shear, as well as yaw misalignment.

Table 5. Overview of average absolute errors and estimated output damage equivalent loads (DELs) under various inflow conditions.

Inflow conditions	Time duration [hrs]	Estimation error [%]			
		M_{TB} Avg. Abs.	$M_{B-25\%}$ Avg. Abs.	M_{TB} DELs	$M_{B-25\%}$ DELs
Clean freestream	11	4.2	2.7	4.3	9.1
Extreme vertical shear	3	6.0	2.4	6.7	7.3
Wake steering via yaw control	2.5	6.2	2.3	0.9	8.0
Waked	2	11.4	5.1	0.9	13.3

3.2.4 Condition monitoring

Next, the measurements of the tower-base and 25%-span blade bending moments were utilized to implement and validate a data-driven a posteriori error correction of the corresponding output equations, following Eq. (11), in order to provide a high-quality prediction of these quantities. In this second scenario, the turbine is permanently equipped with sensors, and the digital shadow provides expected values for these quantities of interest based on the current operational conditions. A CM activity (not discussed or analyzed further in this work) can then be based on the comparison of measurements and predictions, thereby detecting possible anomalies. The quality of the predictions is quantified in terms of the Root Mean Squared Percentage Error (RMSPE), which is commonly used in CM (Liu et al., 2023).

https://doi.org/10.5194/wes-2025-98
Preprint. Discussion started: 17 June 2025

The same dataset presented in Sect. 3.2.2 was used for training, with the sample day allocated for validation. The MATLAB Deep Learning Toolbox (The MathWorks, Inc., 2022) was used to implement and train the NN-based correction term. Following a basic trial-and-error approach, a neural network architecture with a single hidden layer containing 16 neurons was selected. During training, the Polak-Ribiére Conjugate Gradient algorithm (traincgp) and BFGS quasi-Newton backpropagation (trainbfg) yielded the best performance for tower-base and 25%-span blade bending moment, respectively. Notably, the achieved RMSPEs for the training of the tower-base and 25%-span blade bending moments were as low as about 0.8% and 0.9%, respectively.

Figures 12(a) and 12(b) report time histories of the tower-base and 25%-span blade bending moment resultants, respectively. Measurements are shown with a dashed blue line and the corrected ones with a solid green line. Before implementing the a-posteriori error correction, the RMSPE for M_{TB} and $M_{B-25\%}$ were 6.1% and 21.6%, respectively. After data-driven correction, these values dropped to 1.3% and 1.5%, respectively.

Overall, it appears that the proposed data-driven approach is very effective at correcting the output equations, as both slow and fast fluctuations of the two quantities of interest are followed with remarkable accuracy, although it cannot improve the state model.

4 Conclusions

We have presented, verified, and validated with respect to one field dataset a wind turbine digital shadow. Building on a classical Kalman filtering approach, the proposed digital shadow formulation linearizes an existing and trusted aeroservoelastic model to derive the filter-internal linear model. Reusing existing models reduces development time, leverages resources already invested in tuning and validation, increases confidence in the results, and avoids duplication of effort.

However, departing from the existing literature, we have included in the model the tower side-side and the rotor blade DOFs in order to support more general operating conditions, such as the ones deriving from sheared inflows, waked, and yaw-misaligned operation. Since the linearization must now span a much wider solution space than in existing similar approaches, the filter-internal model is scheduled with respect to a number of parameters tasked with representing the main drivers of the turbine response. The rotor as a sensor technology is used to estimate these scheduling parameters in real time during operation from SCADA and blade load measurements.

Testing in a simulation environment showed that the accuracy of the states of the digital shadow generally remains below 10% across all tested conditions. The average absolute error for DELs is in the range of 5%–15%, the larger values being observed in higher ambient turbulence and in waked conditions, as expected. Slightly larger errors (16.1%) were observed for a misaligned turbine, where the complex behavior of the rotor is probably not completely captured by the linearized model. Remarkably, the accuracy of the digital shadow applied to a field dataset was very similar to the one obtained in the simulation environment, even without any ad hoc tuning of the model. However, clear biases were present, which are indicative of the limits of the underlying filter-internal model.

https://doi.org/10.5194/wes-2025-98
Preprint. Discussion started: 17 June 2025

Indeed, the main weakness of a digital shadow is its reliance on a white state-space model. This is invariably affected by errors, which in turn will always limit the quality of the estimates that it can produce. To cope with this issue, we have investigated two alternative ways of augmenting the model with data-driven correction terms, resulting in grey models of greatly improved predictive accuracy.

In particular, the fine-tuned BC approach demonstrated robust performance under complex inflow conditions, including extreme vertical shear, waked, and wake-steering control, during field validation. Despite these challenging scenarios, the errors remained small across all tested cases, further highlighting the reliability and adaptability of the proposed approach.

The bias correction method demonstrated strong performance, lowering the average absolute error from approximately 20% to a range of 2%–11%. Additionally, the average DEL estimation error was reduced to between 1%–13%. These improvements represent a substantial advancement over results reported in the recent literature and highlight the potential of the proposed approach for fatigue analysis, lifetime consumption estimation, and load-aware control strategies. In parallel, the neural correction of the selected outputs of interest also proved highly effective, reducing the load RMSPE from a range of 10%–15% to approximately 1%. This outcome is particularly promising for the application of the digital shadow in CM scenarios.

The approach discussed here can be improved in several ways. For example, other inflow quantities may be necessary to further improve the scheduling of the filter-internal model. One such parameter is veer, which, however, could be readily added to the scheduling parameters, as it can be estimated with the rotor as a sensor technology by expanding the load harmonics to include the 2P (Bertelè et al., 2024). Regarding validation, while the current results are encouraging, it is clear that the proposed approach should be tested on larger field datasets covering a wider range of inflow and operating conditions, as well as different turbine types. In addition, the tuning of the BC correction term could be improved by considering not only wind speed but also variations in vertical and horizontal shear and yaw misalignment, which also require more extensive data.

https://doi.org/10.5194/wes-2025-98
Preprint. Discussion started: 17 June 2025

WIND ENERGY SCIENCE DISCUSSIONS

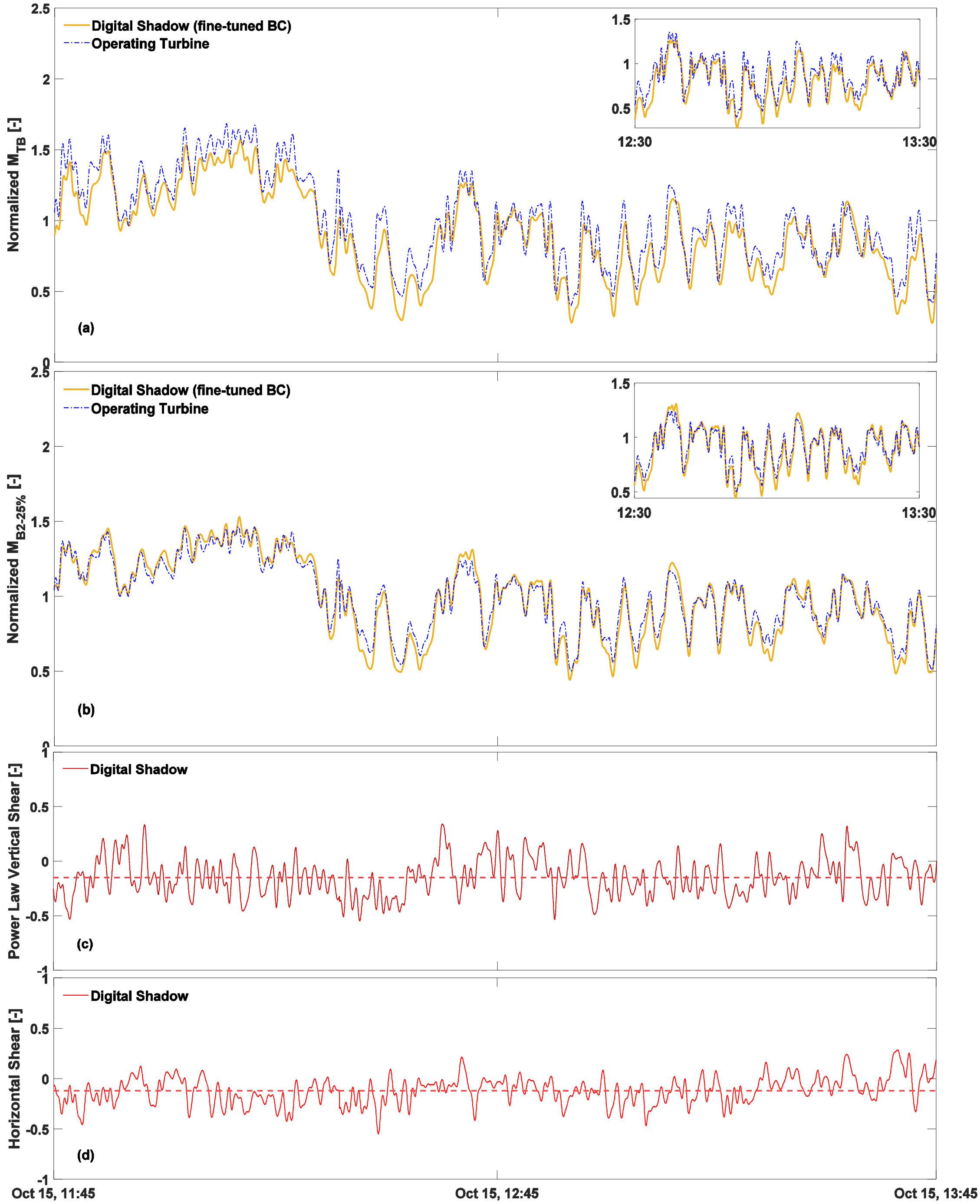

Figure 11. Time histories of the tower-base bending moment **(a)**, blade bending moment at 25% blade span **(b)**, vertical shear **(c)**, and horizontal shears **(d)**. Measurements: dashed blue line; corrected estimates of the digital shadow using fine-tuned BC: solid yellow line. The shears are shown with solid red lines, with an average value marked by red dashed lines. All values have been normalized using the same factor to preserve the confidentiality of the measured turbine data.

https://doi.org/10.5194/wes-2025-98
Preprint. Discussion started: 17 June 2025

Figure 12. Time histories of the tower-base bending moment **(a)** and blade bending moment at 25% blade span **(b)**. Measurements: dashed blue line; corrected estimates of the digital shadow using NN: solid green line. All values have been normalized using the same factor to preserve the confidentiality of the measured turbine data.

https://doi.org/10.5194/wes-2025-98
Preprint. Discussion started: 17 June 2025

Appendix A: Nomenclature

$\mathbf{b}$	Vector of sensor biases
$\mathbf{f}_0$	Static correction force
$\mathbf{i}$	Input vector of the inflow estimator
$\mathbf{p}$	Vector of free network parameters
$\mathbf{q}$	Vector of generalized displacements
$\mathbf{s}$	Vector of scheduling parameters
$\mathbf{u}$	Input vector
$\mathbf{v}$	Vector of generalized velocities
$\mathbf{y}$	Vector of outputs for Kalman innovation
$\mathbf{z}$	Vector of other outputs of interest
ν	Measurement noise vector
ω	Process noise vector
A	Rotor swept area
c	Generic output of the wind inflow characteristic observer
C_p	Power coefficient
d	Displacement
J	Rotor inertia
κ_h	Horizontal shear
M	Bending moment resultant
m	Bending moment component
Q	Torque
R	Rotor radius
V	Wind speed
α	Vertical power-law shear exponent
γ	Misalignment angle
ϵ	Output correction term
θ	Blade pitch angle
λ	Tip speed ratio
ρ	Air density
ψ	Rotor azimuthal position

https://doi.org/10.5194/wes-2025-98
Preprint. Discussion started: 17 June 2025

Ω	Rotor rotational speed
$(\cdot)^E$	Edgewise component
$(\cdot)^F$	Flapwise component
$(\cdot)^{FA}$	Fore-aft component
$(\cdot)^{SS}$	Side-side component
$(\cdot)^{IP}$	In-plane component
$(\cdot)^{OP}$	Out-of-plane component
$(\cdot)^{NN}$	Quantity corrected by a neural network
$(\cdot)_{1c}$	1P cosine component
$(\cdot)_{1s}$	1P sine component
$(\cdot)_{Bi}$	Quantity referred to the ith blade
$(\cdot)_{B-s\%}$	Quantity referred to the $s\%$ spanwise location
$(\cdot)_{TB}$	Quantity referred to the base of the tower
$(\cdot)_E$	Estimated quantity
$(\cdot)_M$	Measured quantity
$(\cdot)_0$	Reference equilibrium condition
$\delta(\cdot)$	Perturbation about a reference equilibrium condition

BEM	Blade element momentum
CFD	Computational fluid dynamics
CM	Condition monitoring
DEL	Damage-equivalent load
DOF	Degree of freedom
FA	Fore-aft
FEM	Finite element method
FFT	Fast Fourier transform
LUT	Look-up table
NN	Neural network
BC	Bias correction
PSD	Power spectral density
RMSPE	Root mean squared percentage error
ROM	Reduced order model
SCADA	Supervisory control and data acquisition
SS	Side-side

TI	Turbulence intensity
WT	Wind turbine

Data availability. All figures and the data used to generate them can be retrieved in Pickle Python and MATLAB formats via https://doi.org/10.5281/zenodo.11519470. The field dataset is the property of eno energy systems GmbH.

Author contributions. CLB and HH developed the formulation of the digital shadow. HH developed the software implementation, performed the numerical simulations, and processed the field dataset. CLB supervised the work. Both authors contributed equally to the interpretation of the results and to the writing of the paper.

Competing interests. At least one of the (co-)authors is a member of the editorial board of *Wind Energy Science*.

Acknowledgements. The technical assistance from Marta Bertelè, Carlo. L Sucameli, Adrien Guilloré, and Abhinav Anand is acknowledged and greatly appreciated. The authors express their gratitude to eno energy systems GmbH, which granted access to the turbine aeroelastic model and to the field dataset.

Financial support. This work has been supported in part by the PowerTracker (FKZ: 03EE2036A), CompactWind II project (FKZ: 0325492G), and Life-Odometer (FKZ: 03EE3037B) projects, which receive funding from the German Federal Ministry for Economic Affairs and Climate Action (BMWK). Additional support has been provided by by the MERIDIONAL project, which receives funding from the European Union's Horizon Europe program under the grant agreement no. 101084216.

https://doi.org/10.5194/wes-2025-98
Preprint. Discussion started: 17 June 2025

References

Abdallah, I., Tatsis, K., and Chatzi, E.: Fatigue assessment of a wind turbine blade when output from multiple aero-elastic simulators are available, Procedia Engineering, 199, 3170–3175, https://doi.org/https://doi.org/10.1016/j.proeng.2017.09.509, x International Conference on Structural Dynamics, EURODYN 2017, 2017.

Anand, A. and Bottasso, C. L.: Reducing Plant-Model Mismatch for Economic Model Predictive Control of Wind Turbine Fatigue by a Data-Driven Approach, in: 2023 American Control Conference (ACC), 979-8-3503-2806-6, pp. 1473–1479, https://doi.org/10.23919/ACC55779.2023.10156501, 2023.

Bangalore, P., Letzgus, S., Karlsson, D., and Patriksson, M.: An artificial neural network-based condition monitoring method for wind turbines, with application to the monitoring of the gearbox, Wind Energy, 20, 1421–1438, https://doi.org/https://doi.org/10.1002/we.2102, 2017.

Bernhammer, L. O., van Kuik, G. A., and De Breuker, R.: Fatigue and extreme load reduction of wind turbine components using smart rotors, Journal of Wind Engineering and Industrial Aerodynamics, 154, 84–95, https://doi.org/https://doi.org/10.1016/j.jweia.2016.04.001, 2016.

Bertelè, M., Bottasso, C. L., and Schreiber, J.: Wind inflow observation from load harmonics: initial steps towards a field validation, Wind Energy Science, 6, 759–775, https://doi.org/10.5194/wes-6-759-2021, 2021.

Bertelè, M., Meyer, P. J., Sucameli, C. R., Fricke, J., Wegner, A., Gottschall, J., and Bottasso, C. L.: The rotor as a sensor – Observing shear and veer from the operational data of a large wind turbine, Wind Energy Science, 9, 1419–1429, https://doi.org/10.5194/wes-9-1419-2024, 2024.

Boorsma, K., Greco, L., and Bedon, G.: Rotor wake engineering models for aeroelastic applications, Journal of Physics: Conference Series, 1037, 062 013, https://doi.org/10.1088/1742-6596/1037/6/062013, 2018.

Bottasso, C., Campagnolo, F., Croce, A., and Tibaldi, C.: Optimization-based study of bend–twist coupled rotor blades for passive and integrated passive/active load alleviation, Wind Energy, 16, 1149–1166, https://doi.org/https://doi.org/10.1002/we.1543, 2013.

Bottasso, C. L., Chang, C.-S., Croce, A., Leonello, D., and Riviello, L.: Adaptive planning and tracking of trajectories for the simulation of maneuvers with multibody models, Computer Methods in Applied Mechanics and Engineering, 195, 7052–7072, https://doi.org/https://doi.org/10.1016/j.cma.2005.03.011, multibody Dynamics Analysis, 2006.

Branlard, E., Giardina, D., and Brown, C. S. D.: Augmented Kalman filter with a reduced mechanical model to estimate tower loads on a land-based wind turbine: a step towards digital-twin simulations, Wind Energy Science, 5, 1155–1167, https://doi.org/10.5194/wes-5-1155-2020, 2020a.

Branlard, E., Jonkman, J., Dana, S., and Doubrawa, P.: A digital twin based on OpenFAST linearizations for real-time load and fatigue estimation of land-based turbines, Journal of Physics: Conference Series, 1618, 022 030, https://doi.org/10.1088/1742-6596/1618/2/022030, 2020b.

Branlard, E., Jonkman, J., Brown, C., and Zhang, J.: A digital twin solution for floating offshore wind turbines validated using a full-scale prototype, Wind Energy Science, 9, 1–24, https://doi.org/10.5194/wes-9-1-2024, 2024a.

Branlard, E., Jonkman, J., Lee, B., Jonkman, B., Singh, M., Mayda, E., and Dixon, K.: Improvements to the Blade Element Momentum Formulation of OpenFAST for Skewed Inflows, Journal of Physics: Conference Series, 2767, 022 003, https://doi.org/10.1088/1742-6596/2767/2/022003, 2024b.

Branlard, E. S. P.: Flexible multibody dynamics using joint coordinates and the Rayleigh-Ritz approximation: The general framework behind and beyond Flex, Wind Energy, 22, 877–893, https://doi.org/https://doi.org/10.1002/we.2327, 2019.

Burden, F. and Winkler, D.: Bayesian Regularization of Neural Networks, pp. 23–42, Humana Press, Totowa, NJ, ISBN 978-1-60327-101-1, https://doi.org/10.1007/978-1-60327-101-1_3, 2009.

Chen, J., Pan, J., Li, Z., Zi, Y., and Chen, X.: Generator bearing fault diagnosis for wind turbine via empirical wavelet transform using measured vibration signals, Renewable Energy, 89, 80–92, https://doi.org/https://doi.org/10.1016/j.renene.2015.12.010, 2016.

Chui, C. K. and Chen, G.: Kalman Filtering with Real-Time Applications, Springer, 1999.

Coleman, R. P. and Feingold, A. M.: Theory of Self-Excited Mechanical Oscillations of Helicopter Rotors with Hinged Blades, Technical Report NACA TN 1351, NACA, https://digital.library.unt.edu/ark:/67531/metadc56181/m2/1/high_res_d/19930084623.pdf, last accessed: 07 June 2024, 1958.

Dimitrov, N., Kelly, M. C., Vignaroli, A., and Berg, J.: From wind to loads: wind turbine site-specific load estimation with surrogate models trained on high-fidelity load databases, Wind Energy Science, 3, 767–790, https://doi.org/10.5194/wes-3-767-2018, 2018.

Drécourt, J.-P., Madsen, H., and Rosbjerg, D.: Bias aware Kalman filters: Comparison and improvements, Advances in Water Resources, 29, 707–718, https://doi.org/https://doi.org/10.1016/j.advwatres.2005.07.006, 2006.

eno energy GmbH: https://www.eno-energy.com/, eno energy GmbH, last access on 15.02.2024.

Evans, M., Han, T., and Shuchun, Z.: Development and validation of real time load estimator on Goldwind 6 MW wind turbine, Journal of Physics: Conference Series, 1037, 032 021, https://doi.org/10.1088/1742-6596/1037/3/032021, 2018.

Grewal, M. S. and Andrews, A. P.: Kalman Filtering: Theory and Practice with MATLAB, John Wiley & Sons, Inc., 2008.

Grewal, M. S. and Andrews, A. P.: Kalman Filtering: Theory and Practice Using Matlab, John Wiley & Sons, Inc., https://doi.org/https://doi.org/10.1002/9781118984987, 2014.

Guilloré, A., Campagnolo, F., and Bottasso, C. L.: A control-oriented load surrogate model based on sector-averaged inflow quantities: capturing damage for unwaked, waked, wake-steering and curtailed wind turbines, Journal of Physics: Conference Series, 2767, 032 019, https://doi.org/10.1088/1742-6596/2767/3/032019, 2024.

Hoghooghi, H.: Load Alleviation on Multi-Megawatt Wind Turbines Based on Measured Dynamic Response of Wind Turbine, Doctoral thesis, ETH Zurich, Zurich, https://doi.org/10.3929/ethz-b-000492802, 2021.

Hoghooghi, H., Chokani, N., and Abhari, R.: Effectiveness of individual pitch control on a 5MW downwind turbine, Renewable Energy, 139, 435–446, https://doi.org/https://doi.org/10.1016/j.renene.2019.02.088, 2019a.

Hoghooghi, H., Chokani, N., and Abhari, R. S.: Enhanced Yaw Stability of Downwind Turbines, Journal of Physics: Conference Series, 1356, 012 020, https://doi.org/10.1088/1742-6596/1356/1/012020, 2019b.

Hoghooghi, H., Chokani, N., and Abhari, R.: Optical measurements of multi-megawatt wind turbine dynamic response, Journal of Wind Engineering and Industrial Aerodynamics, 206, 104 214, https://doi.org/https://doi.org/10.1016/j.jweia.2020.104214, 2020a.

Hoghooghi, H., Chokani, N., and Abhari, R. S.: Individual Blade Pitch Control for Extended Fatigue Lifetime of Multi-Megawatt Wind Turbines, Journal of Physics: Conference Series, 1618, 022 008, https://doi.org/10.1088/1742-6596/1618/2/022008, 2020b.

Hoghooghi, H., Chokani, N., and Abhari, R. S.: A novel optimised nacelle to alleviate wind turbine unsteady loads, Journal of Wind Engineering and Industrial Aerodynamics, 219, 104 817, https://doi.org/https://doi.org/10.1016/j.jweia.2021.104817, 2021.

Hoghooghi, H., Bertelè, M., Anand, A., and Bottasso, C. L.: A wind turbine digital shadow with tower and blade degrees of freedom - Preliminary results and comparison with a simple tower fore-aft model, Journal of Physics: Conference Series, 2767, 032 026, https://doi.org/10.1088/1742-6596/2767/3/032026, 2024.

IEA3.37MW(2023): https://github.com/IEAWindTask37/IEA-3.4-130-RWT/tree/master, the onshore reference wind turbine developed within IEA Wind Task 37, last access on 01.08.2023.

eawe european academy of wind energy
Open Access WIND ENERGY SCIENCE DISCUSSIONS

IEC: IEC 61400-1 Wind turbines: Design requirements, International Electrotechnical Commision, 2005.

Iliopoulos, A., Shirzadeh, R., Weijtjens, W., Guillaume, P., Hemelrijck, D. V., and Devriendt, C.: A modal decomposition and expansion approach for prediction of dynamic responses on a monopile offshore wind turbine using a limited number of vibration sensors, Mechanical Systems and Signal Processing, 68-69, 84–104, https://doi.org/https://doi.org/10.1016/j.ymssp.2015.07.016, 2016.

Jacquelin, E., Bennani, A., and Hamelin, P.: Force reconstruction: analysis and regularization of a deconvolution problem, Journal of Sound and Vibration, 265, 81–107, https://doi.org/https://doi.org/10.1016/S0022-460X(02)01441-4, 2003.

Jonkman, J. and Shaler, K.: FAST.Farm User's Guide and Theory Manual, Tech. Rep. NREL/TP-5000-78485, National Renewable Energy Laboratory (NREL), 2021.

Jonkman, J. M., Wright, A. D., Hayman, G. J., and Robertson, A. N.: Full-System Linearization for Floating Offshore Wind Turbines in OpenFAST, ASME 2018 1st International Offshore Wind Technical Conference, V001T01A028, https://doi.org/10.1115/IOWTC2018-1025, 2018.

Kim, K.-H., Bertelè, M., and Bottasso, C. L.: Wind inflow observation from load harmonics via neural networks: A simulation and field study, Renewable Energy, 204, 300–312, https://doi.org/https://doi.org/10.1016/j.renene.2022.12.051, 2023.

Liu, J., Wang, X., Xie, F., Wu, S., and Li, D.: Condition monitoring of wind turbines with the implementation of spatio-temporal graph neural network, Engineering Applications of Artificial Intelligence, 121, 106 000, https://doi.org/https://doi.org/10.1016/j.engappai.2023.106000, 2023.

Loew, S. and Bottasso, C. L.: Lidar-assisted model predictive control of wind turbine fatigue via online rainflow counting considering stress history, Wind Energy Science, 7, 1605–1625, https://doi.org/10.5194/wes-7-1605-2022, 2022.

Matlab: Deep Learning Toolbox, https://www.mathworks.com/help/deeplearning/, last accessed 27 July 2024, 2023.

Mendez Reyes, H., Kanev, S., Doekemeijer, B., and van Wingerden, J.-W.: Validation of a lookup-table approach to modeling turbine fatigue loads in wind farms under active wake control, Wind Energy Science, 4, 549–561, https://doi.org/10.5194/wes-4-549-2019, 2019.

Natarajan, A.: Damage equivalent load synthesis and stochastic extrapolation for fatigue life validation, Wind Energy Science, 7, 1171–1181, https://doi.org/10.5194/wes-7-1171-2022, 2022.

Noppe, N., Iliopoulos, A., Weijtjens, W., and Devriendt, C.: Full load estimation of an offshore wind turbine based on SCADA and accelerometer data, Journal of Physics: Conference Series, 753, 072 025, https://doi.org/10.1088/1742-6596/753/7/072025, 2016.

NREL Forum: https://forums.nrel.gov/t/openfast-linearization-of-nrel-5mw-onshore-turbine/2573, openFAST: Linearization of NREL 5MW Onshore Turbine, last access on 01.08.2023, 2023.

Olatunji, O. O., Adedeji, P. A., Madushele, N., and Jen, T.-C.: Overview of Digital Twin Technology in Wind Turbine Fault Diagnosis and Condition Monitoring, in: 2021 IEEE 12th International Conference on Mechanical and Intelligent Manufacturing Technologies (ICMIMT), pp. 201–207, https://doi.org/10.1109/ICMIMT52186.2021.9476186, 2021.

OpenFAST, 2024: https://github.com/OpenFAST/openfast/, openFAST, last access on 29.07.2024.

Pacheco, J., Pimenta, F., Guimarães, S., Castro, G., Álvaro Cunha, Matos, J. C., and Magalhães, F.: Experimental evaluation of fatigue in wind turbine blades with wake effects, Engineering Structures, 300, 117 140, https://doi.org/https://doi.org/10.1016/j.engstruct.2023.117140, 2024.

Schreiber, J., Bottasso, C. L., and Bertelè, M.: Field testing of a local wind inflow estimator and wake detector, Wind Energy Science, 5, 867–884, https://doi.org/10.5194/wes-5-867-2020, 2020a.

Schreiber, J., Bottasso, C. L., and Bertelè, M.: Field testing of a local wind inflow estimator and wake detector, Wind Energy Science, 5, 867–884, https://doi.org/10.5194/wes-5-867-2020, 2020b.

https://doi.org/10.5194/wes-2025-98
Preprint. Discussion started: 17 June 2025

Schröder, L., Dimitrov, N. K., Verelst, D. R., and Sørensen, J. A.: Wind turbine site-specific load estimation using artificial neural networks calibrated by means of high-fidelity load simulations, Journal of Physics: Conference Series, 1037, 062 027, https://doi.org/10.1088/1742-6596/1037/6/062027, 2018.

Sepasgozar, S. M. E.: Differentiating Digital Twin from Digital Shadow: Elucidating a Paradigm Shift to Expedite a Smart, Sustainable Built Environment, Buildings, 11, https://doi.org/10.3390/buildings11040151, 2021.

Song, Z., Hackl, C. M., Anand, A., Thommessen, A., Petzschmann, J., Kamel, O., Braunbehrens, R., Kaifel, A., Roos, C., and Hauptmann, S.: Digital Twins for the Future Power System: An Overview and a Future Perspective, Sustainability, 15, 2023.

Surucu, O., Gadsden, S. A., and Yawney, J.: Condition Monitoring using Machine Learning: A Review of Theory, Applications, and Recent Advances, Expert Systems with Applications, 221, 119 738, https://doi.org/https://doi.org/10.1016/j.eswa.2023.119738, 2023.

The MathWorks, Inc.: MATLAB and Statistics Toolbox Release [2022b], Natick, MA, 2022.

TurbSim(2023): https://github.com/old-NWTC/TurbSim, turbSim, last access on 01.08.2023.

Vettori, S., Di Lorenzo, E., Peeters, B., and Chatzi, E.: A virtual sensing approach to operational modal analysis for wind turbine blades, 2020.

Wan, E. and Van Der Merwe, R.: The unscented Kalman filter for nonlinear estimation, pp. 153–158, https://doi.org/10.1109/ASSPCC.2000.882463, 2000.

Wu, P., Liu, Y., Ferrari, R. M., and van Wingerden, J.-W.: Floating offshore wind turbine fault diagnosis via regularized dynamic canonical correlation and fisher discriminant analysis, IET Renewable Power Generation, 15, 4006–4018, https://doi.org/https://doi.org/10.1049/rpg2.12319, 2021.

Ziegler, L., Smolka, U., Cosack, N., and Muskulus, M.: Brief communication: Structural monitoring for lifetime extension of offshore wind monopiles: can strain measurements at one level tell us everything?, Wind Energy Science, 2, 469–476, https://doi.org/10.5194/wes-2-469-2017, 2017.